Qiu Haijun (Orcid ID: 0000-0003-0263-0025)

Automated extraction of mining-induced ground fissures using deep learning and object-based image classification

Author Manuscript

Abstract: Accurate extraction of ground fissures caused by intense coal mining has the potential to significantly improve the efficiency of environmental monitoring in mining areas. However, the extraction results using previous methods have often exhibited issues of discontinuity and substantial deviation from ground truth data, resulting in low extraction accuracy. In this study, a novel approach, ENVINet5-OBIC, for extracting ground fissures in mining areas is proposed, which integrates object-based image classification (OBIC) with the pixel-based deep learning model ENVINet5. ENVINet5-OBIC uses OBIC to segment high-resolution unmanned aerial vehicle (UAV) images across different scales, effectively considering shape, texture, and correlative information between adjacent pixels. Furthermore, by utilizing homogeneous objects as building blocks, it establishes a deep learning model for the automated extraction of ground fissures. Experimental results show that ENVINet5-OBIC performs better when compared to OBIC, U-Net, PSPNet, and ENVINet5 methods in terms of continuity, accuracy, and error reduction. In addition, the ground fissure area extracted by ENVINet5-OBIC closely aligns with ground truth data. This study provides a more effective method for automatic extraction of ground fissures, which improves the efficiency of environmental monitoring in mining areas.

Keywords: Ground fissure; Automatic extraction; Deep learning; Object-based image classification; UAV image

This is the author manuscript accepted for publication and has undergone full peer review but has not been through the copyediting, typesetting, pagination and proofreading process, which may lead to differences between this version and the Version of Record. Please cite this article as doi: 10.1002/esp.5824

This article is protected by copyright. All rights reserved.

Author Manuscript

1. Introduction

The intensive extraction of underground coal resources can disrupt stress patterns within overlying rock layers, resulting in surface collapses and the formation of ground fissures (Hu & Wang, 2014; Malinowska & Hejmanowski, 2016; Qiu et al., 2022; Ma et al., 2023). These ground fissures may lead to disturbances in vegetation and cultivated land, potentially posing a severe threat to residents' well-being and giving rise to an array of social and economic challenges in mining regions (Kong et al., 2016; Chen et al., 2020; He et al., 2020; Pei et al., 2023; Liu et al., 2024). Therefore, accurate identification and extraction of ground fissures is crucial to improve the efficiency of environmental monitoring and develop effective prevention measures for mining in vulnerable ecosystems.

Traditional methods of acquiring ground fissure information are mainly based on measurements using GPS and other instruments (Zhao et al., 2013; Li et al., 2017; Zhou et al., 2019). These methods are time-consuming and labor-intensive, often leading to delays in obtaining timely information on ground fissure evolution, thus affecting prompt analysis and assessment (Zhao et al., 2013, 2021). With the improvement of sensor resolution, remote sensing technology has been widely used in the field of geological hazard investigation and monitoring. For example, Synthetic Aperture Radar Interferometry (InSAR) is used for the detection and monitoring of large slope deformations (Michoud et al., 2016; Ye et al., 2024) and the prediction of catastrophic slope failures (Carlà et al., 2019; Zhou et al., 2022). High-resolution unmanned aerial vehicles (UAV) images have been used to extract ground fissures from coal mining subsidence (Yang et al., 2022) and loess areas (Jia et al., 2021). Zhao et al. (2021) used UAV and infrared thermal imager to identify mining-induced ground fissures. Most ground fissures are only a few centimeter in width, and it is

Author Manuscript

difficult to identify them using optical satellite remote sensing data (Liu et al., 2019; Yang et al., 2019; Fu et al., 2021). Fortunately, UAV can deliver images at the scale of centimeters, which can fully display distribution patterns of ground fissures, and hence UAV imagery has been used to identify ground objects (Jia et al., 2021; Zhao et al., 2021; Jiang et al., 2022; Yang et al., 2022; Yang et al., 2023).

Ground fissure extraction methods involving UAV images mainly include visual interpretation, threshold segmentation, edge detection, and machine learning. While visual interpretation is a classical method, it is of low efficiency and requires substantial human resources and expertise. Threshold segmentation is very sensitive to noise (Kheradmandi and Mehranfar, 2022), especially when the spectral signatures of the object and the background are very similar as it this complicates the identification of universal thresholds. In contrast, automated extraction techniques like edge detection and machine learning have been extensively applied in fissure extraction related to, for example, roads (Zhang et al., 2019; Fei et al., 2020), bridges (Zhang et al., 2016, 2018; Perry et al., 2020; Zollini et al., 2020), and landslides (Stumpf et al., 2013; Qu et al., 2021; Wang et al., 2022). The purpose of edge detection is to identify points where brightness changes across the digital images. Common edge detection operators include Sobel, Laplacian, and Canny (Zhang et al., 2019; Nnolim, 2020). While Sobel works well in the processing of gray gradient and noisy images, it is not suitable for edge positioning or edges of more than one pixel. Nevertheless, it has been successfully applied in edge detection of low precision (Tian et al., 2021; Kong et al., 2023). Laplacian is sensitive to noise and rarely used for edge detection, while Canny is not easily disturbed by noise and can detect true weak edges; however, some studies have confirmed that it has not achieved satisfactory results in extracting ground fissures in mining areas (Jiang et al., 2022; Yang et al.,

Author Manuscript

2022). Furthermore, vegetation contours are easily misclassified as edges, resulting in poor generalization performance. Machine learning primarily involves learning and extracting features from annotated samples that are used to predict and categorize unlabeled samples (Parker et al., 2011; Daniel et al., 2012; Cheng et al., 2013; Chen et al., 2018; Zhang et al., 2020; Ye et al., 2022). Traditional machine learning networks tend to be shallow, relying heavily on labeled samples, and are susceptible to errors.

Deep learning excels at capturing intricate features of objects and has reached remarkable levels of performance, encompassing tasks like semantic segmentation (Andres et al., 2018; Ji et al., 2020; Du et al., 2021; Yuan et al., 2023), object detection (Ammour et al., 2017; Bhowmick et al., 2020; Kaur & Singh, 2022; Yu et al., 2022), and image classification (Zhang et al., 2011; Chan et al., 2015). However, deep learning methods available for ground fissures extraction mainly classify spectral features of images based the spectral information of a single pixel. Either adjacent pixels of the same object will be divided into different categories based on spectral differences or adjacent pixels of different objects will be divided into the same category based on spectral similarities. In contrast, object-based image classification (OBIC) takes adjacent pixels with the same or similar features as a homogeneous object, and homogeneous objects of different sizes replace pixels as the basic unit of image classification. In the classification process, a broad range of information is considered for each object including spectral signature, shape, texture, shadow, and spatial position, which describes the semantic relation between objects and can improve the recognition accuracy (Lu et al., 2011, 2020; Stumpf & Kerle, 2011; Eeckhaut et al., 2012; Martha et al., 2012; Hölbling et al., 2019). OBIC has been widely used in image classification of high-resolution images to overcome the shortcomings of pixel-based classification (Blaschke et al., 2014).

Author Manuscript

This research proposes the ENVINet5-OBIC approach, which combines the deep learning model ENVINet5 with OBIC. The UAV image is segmented by OBIC, and then the ground fissure datasets are created by manually marking the object, providing a training set (TS) and a verification set (VS). The label raster is extracted from these datasets, and the deep learning model is constructed to automatically extract the fissures. To verify the feasibility of the proposed method, the extraction results of ground fissures are compared with those using OBIC and ENVINet5.

2. Study area and datasets

2.1. Study area

Zichang County is located in the north of Yan'an, Shaanxi Province, China. It sits within the hinterland of the Loess Plateau, positioned between 109°11'58"E ~ 110°01'22"E, and 36°59'30"N ~ 37°30'00"N (Figure 1a). The county spans approximately 72 km from east to west and 56 km from north to south, covering a total area of 2405 km^2. Elevations gradually drop from 1564 m in the northwest to 906 m in the southeast. The landscape is characterized by the typical undulating hilly ridges and intricate gullies of the Loess Plateau (Figure 1b). The region is intersected by the three rivers Qingjian, Wuding, and Yanhe. The prevailing climate is semi-arid continental monsoon with notable temperature fluctuations. The mean annual temperature is 9.1℃, with a mean annual precipitation of 514.7 mm and a frost-free period spanning 175 days. The region is known for its abundant coal resources, but mining activities often disrupt the geological equilibrium, leading to a cascade of ground fissure-related incidents that threaten ecosystems and the safety of the coal mines.

The study area of 0.459 km^2 within the coal mining region was selected because of the many ground fissures (Figure 1c-k). Elevations range from 1126 to 1301 m, and

slopes range from 1.0° and 44.6°. The vegetation consists of mainly shrubs and grasses with scattered trees.

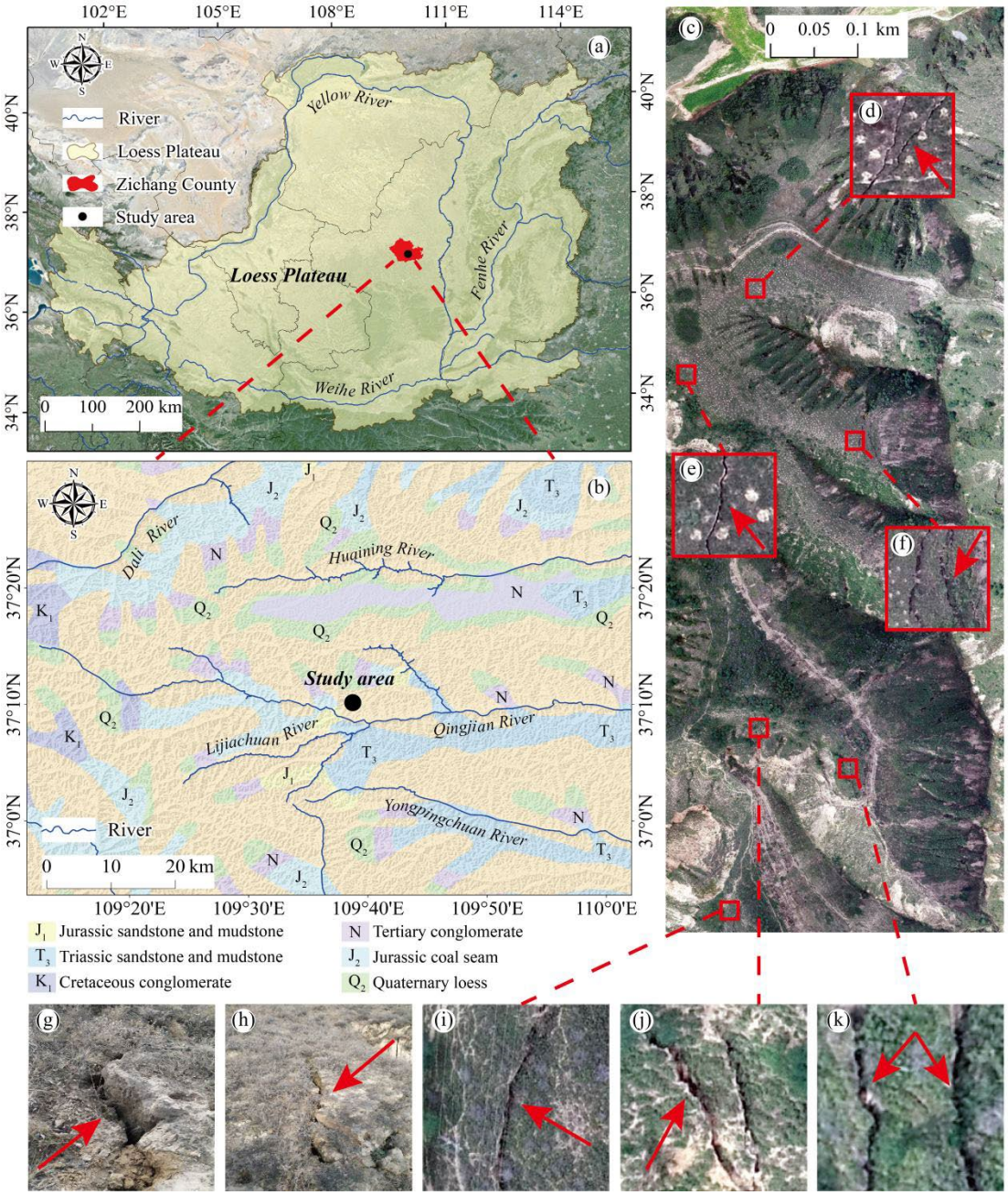


FIGURE 1 (a) The study area lies within Zichang County in the Loess Plateau of China. (b) Geological map of the study area. (c) UAV image of the study area with field investigation sites. (d)-(k) Field investigation sites with ground fissures.

Author Manuscript

Author Manuscript

2.2. Data preparation

A small multi-rotor DJI PHANTOM 4 was used to gather imagery at high resolution of 9.2 cm of surface ground fissures on 5 September 2020. The UAV has a FC6310R camera and flies at an altitude of 270 m at a speed of 7.9 m/s. A total of 30 ground control points (GCPs) were set up, and their locations were obtained using a real-time kinematic global positioning system (RTK-GPS) with an absolute accuracy of 0.02 m and a root-mean-square error (RMSE) of 1.01 cm in the X, 0.49 cm in the Y, and 3.35 cm in the Z directions. Orthophotos with a resolution of 0.092 m were generated using Pix4Dmapper software. The UAV imagery revealed that ground fissures are distributed across flat and ridge areas as well as areas with lush vegetation. To mark the ground fissures, the UAV images were annotated manually and cross-verified using field observations, leading to the creation of the final ground fissure datasets. Datasets were then split into TS and VS subsets. To improve the robustness and generalization ability of the deep learning model and to avoid overfitting that results from an insufficient sample size, data augmentation was performed, including data flipping, rotation, and translation.

3. Method

Three methods were used to extract the ground fissures in the coal mining region from high-resolution UAV imagery (Figure 2). (1) OBIC: The images undergo multi-resolution segmentation; Region-of-Interest (ROI) tools are used to select ground fissure samples; the example-based OBIC is utilized to extract ground fissures. (2) ENVINet5: Ground fissure samples are manually marked on the images, generating a label raster; ENVINet5 is constructed to extract ground fissures. (3) ENVINet5-OBIC: After multi-resolution segmentation, ground fissure samples are manually marked on the images; a new label raster is generated to build the deep

learning model to extract ground fissures. Finally, extraction results are compared using a performance assessment.

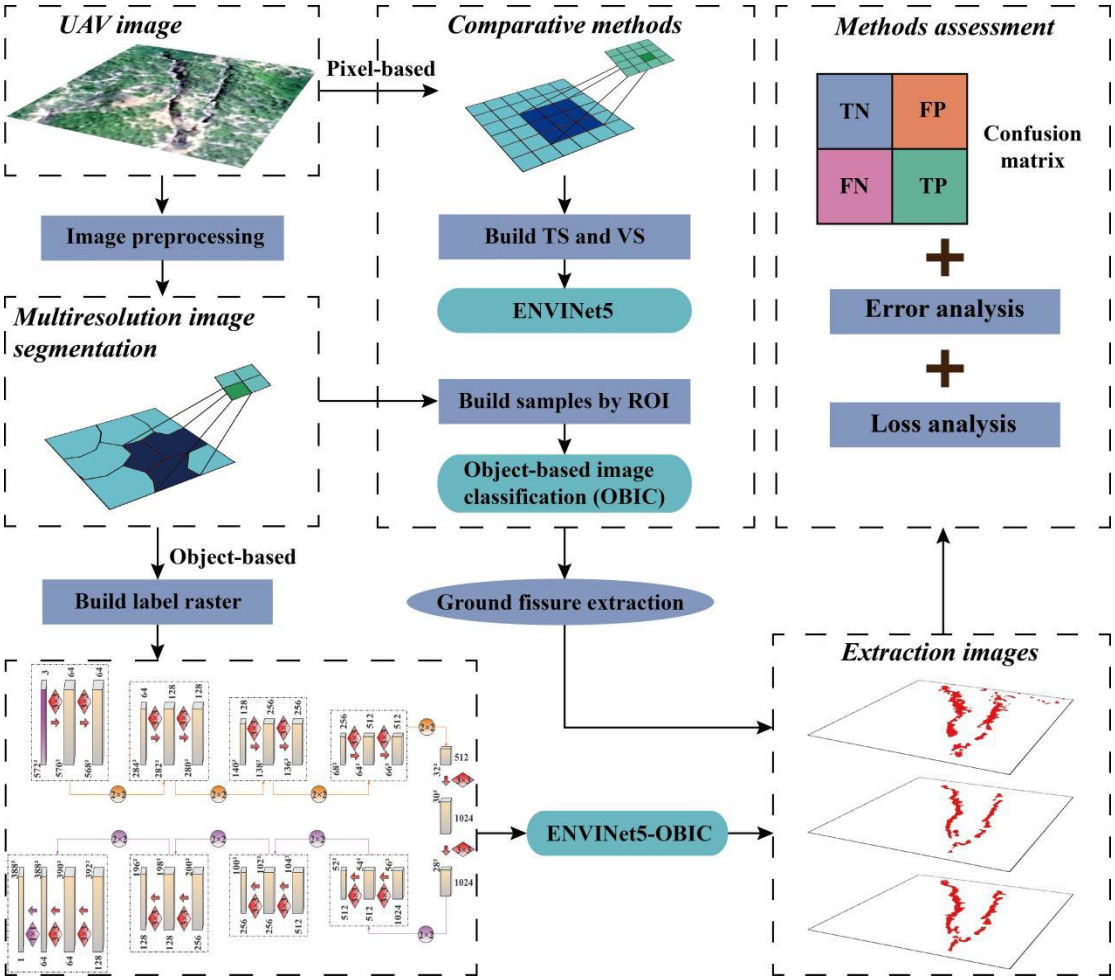


FIGURE 2 Workflow of ground fissures extraction.

3.1. ENVINet5 model

The ENVINet5 model, developed by ESRI based on the TensorFlow deep learning framework, follows an encoder-decoder architecture that is based on using a mask to classify every pixel in the remote sensing images (Ronneberger et al., 2015; Zhang et al., 2020). In addition, the framework uses convolutional neural network (CNN) to find spatial and spectral patterns in the image pixels that match with the provided training data. ENVINet5 offers exceptional flexibility, portability, and performance optimization capabilities. The model's architecture consists of three

Author Manuscript

main components: downsampling, upsampling, and jump connections (Figure 3). TensorFlow is a symbolic math system based on data flow programming, and it is widely used to program various machine learning algorithms (Janardhanan, 2020; Zhang et al., 2020). In this study, the patch size of the model had to be defined, where the patch is a small picture introduced for training purposes. A patch size of 256 was selected, considering computational efficiency and predictive impact. Other parameter values were determined through randomized parameter experiments, where epochs of 25 were established. The number of patches in each epoch was limited to 300. Additional model settings included: solid distance at 13.75, blur distance at 2.23, class weight at 1.37, and loss weight at 0.063.

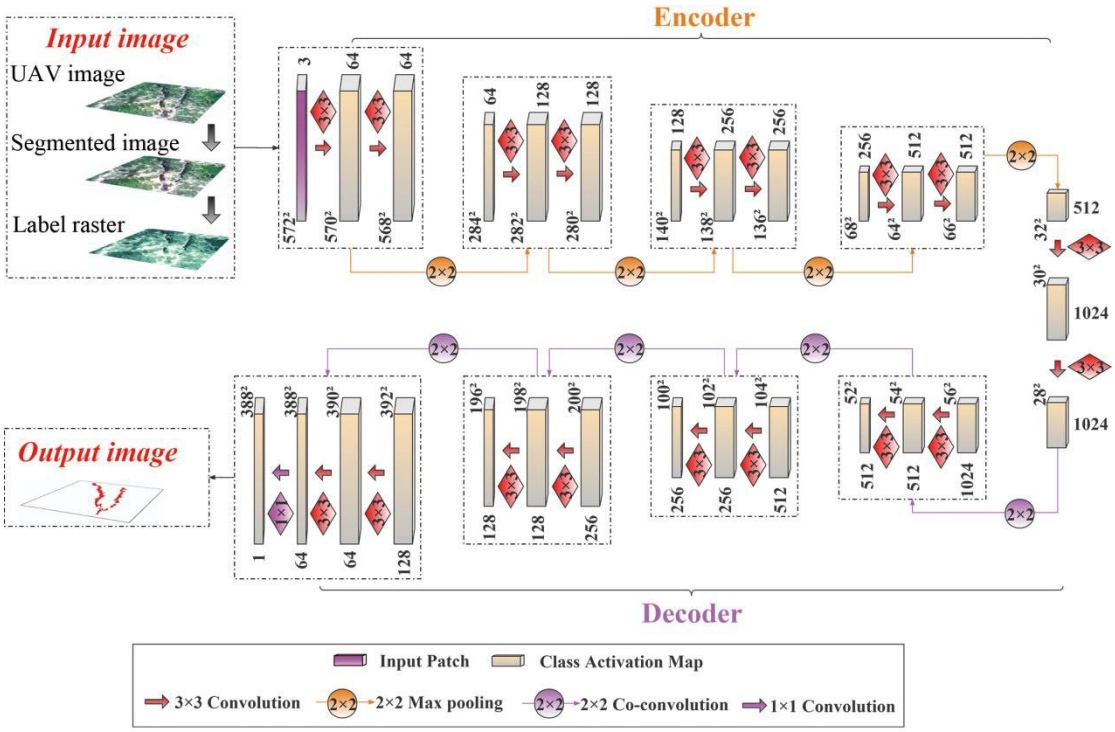


FIGURE 3 Deep learning model architecture.

3.2. Example-based OBIC

The ENVINET5-OBIC proposed in this study was generated by combining OBIC and ENVINet5. OBIC was used for the segmentation of the UAV images with

Author Manuscript

the best threshold. It involves the grouping of similar pixels into homogeneous objects that serve as the basic units for image classification and information extraction. OBIC uses geometric and semantic information, shape, texture, and topological relations of objects, and can obtain image classification results of higher accuracy than traditional pixel-based classification methods (Lu et al., 2011, 2020; Stumpf & Kerle, 2011; Eeckhaut et al., 2012; Martha et al., 2012; Hölbling et al., 2019). The OBIC-derived segmentation image was then used to label object samples to construct a label raster as input for ENVINet5. After the multi-resolution image segmentation according to the appropriate scale, ROI was used to select the samples of objects, while the support vector machine (SVM) model was used to achieve the object-based image classification. SVM is a machine learning algorithm based on structural risk minimization criteria, which is suitable for a high-dimensional feature space and statistical learning using a small sample; it has strong anti-noise ability (Cheng et al., 2013).

3.3. Accuracy assessment

Various evaluation metrics were employed to assess the extraction performance, including overall accuracy (OA), Kappa coefficient (KC), precision, recall, F1-score, and Mean Intersection over Union (MIoU) (Landis & Koch, 1977; Sujatha & Selvathi, 2015; He et al., 2021). OA represents the ratio of correct predictions to the total number of predictions. In contrast, precision is the proportion of correctly classified pixels to the total number of pixels in a category. Recall indicates the proportion of the number of correctly classified pixels to the actual pixels in the class. The F1-score is a comprehensive evaluation index that is the harmonic average of precision and recall. These assessment indices were calculated using a confusion matrix that includes metrics like true positive (TP), true negative (TN), false positive (FP), and

Author Manuscript

false negative (FN) (Fawcett, 2006). TP and TN are the number of accurately classified positive and negative samples, respectively; conversely, FP and FN are the number of incorrectly classified positive and negative samples, respectively. In addition, performance was compared using commission error (CE), omission error (OE), and Loss function. The Loss function estimates the level of inconsistency between predictions and actual outcomes. The smaller the loss, the better the training effect, and the stronger the robustness of the model.

4. Results

4.1. Optimal scale selection of OBIC

The selection of optimal scale has a profound influence on the classification results of OBIC. In this study, the Estimation of Scale Parameter (ESP) tool (Drăguţ et al., 2014) was used to obtain the optimal segmentation scale. ESP is a bottom-up iterative segmentation tool at multiple scales that calculates the Local Variance (LV) of the homogeneity of image objects under different segmentation scale parameters. At the same time, Rate of Change (ROC) was introduced to amplify the local variance mutation and determine the rationality of the segmentation effect. When the local change rate peaks, the segmentation scale is ideal. By previewing the segmentation impact, the merging threshold is established at 30. using ESP, the candidate segmentation scales were set at 30, 40, and 50. To screen out the optimal segmentation scale, the extraction results of ground fissures at the candidate scales were compared (Figure 4). They showed that the location and shape of ground fissures can be accurately identified using the candidate segmentation scales; however, ground fissures with weaker spectral features were not identified at segmentation scales of 30 and 50, resulting in discontinuity in the extraction results. Setting the segmentation scale at 40 avoided discontinuity, and results were most consistent with

Author Manuscript

the ground truth.

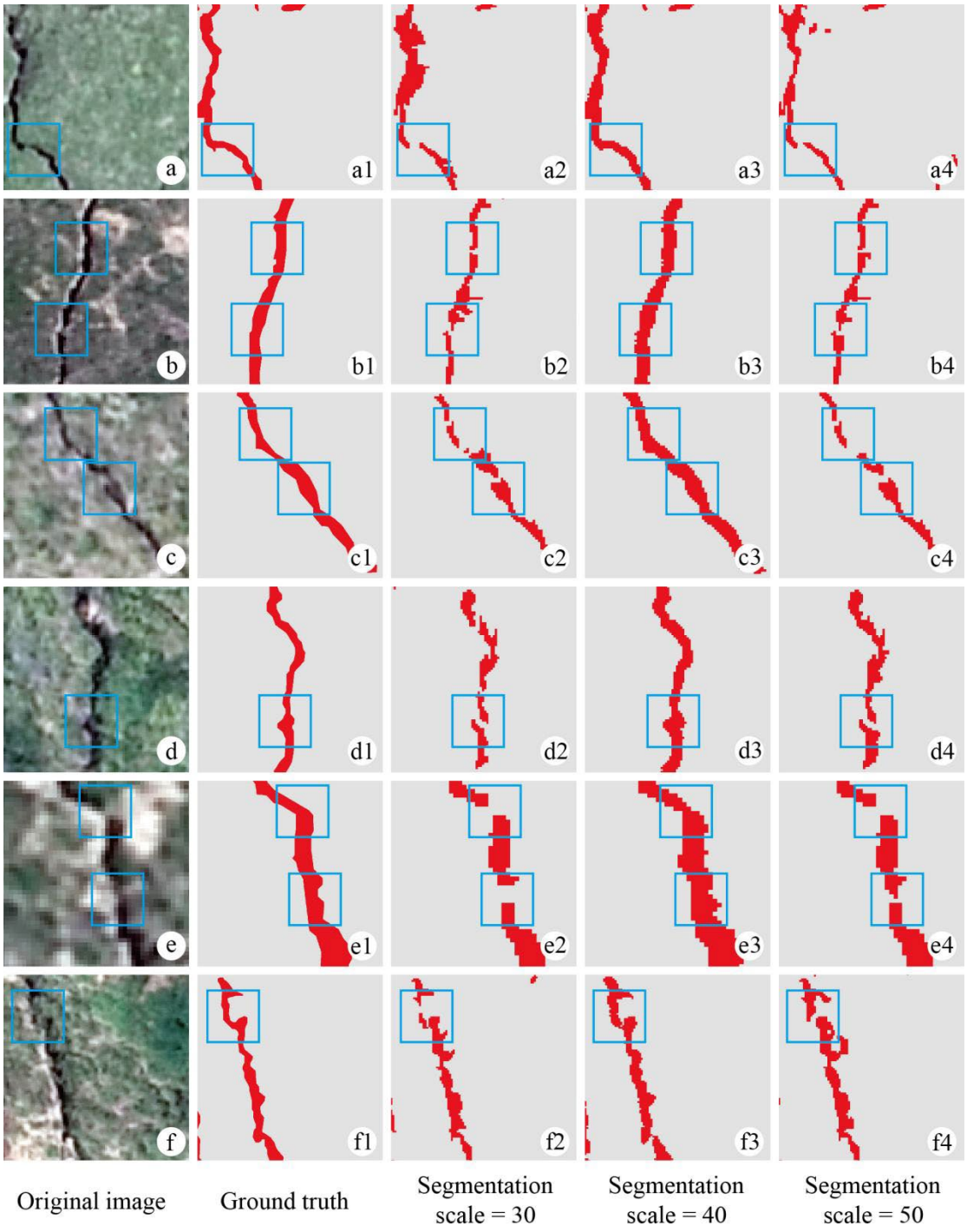


FIGURE 4 Ground fissures extraction results using candidate segmentation scales.

The candidate segmentation scales were used to assess the performance of ground fissure extraction methods. ENVINet5-OBIC with a segmentation scale of 40 achieved the best results: an OA of 0.988, KC of 0.826, Recall of 0.952, F1-score of

Author Manuscript

0.832, and MIoU of 0.850. The error analysis showed that this method achieved the smallest CE of 0.23 and OE of 0.02. Therefore, the final optimal segmentation scale was set at 40.

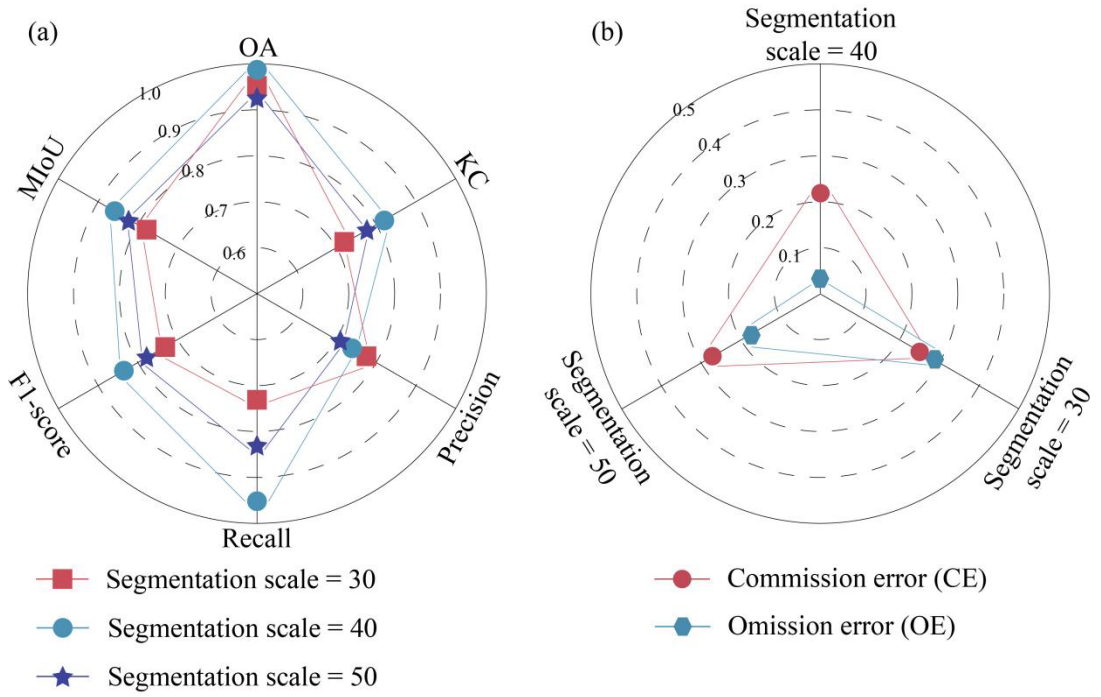


FIGURE 5 Performance of the ENVINet5-OBIC method with candidate segmentation scales in ground fissures extraction. (a) Accuracy assessment. (b) CE and OE analyses.

4.2. Ground fissure extraction on verification set

The VS can be used to verify the reliability and applicability of the proposed method (Figure 6). OBIC was successful in extracting the general outline of ground fissures when the ground objects are relatively simple (Figure 6). However, results were not satisfactory for more complex ground objects. When the width of the extracted ground fissures was larger than in the ground truth data, many shadows were misclassified as ground fissures, resulting in a distinct jagged pattern. Ground fissures are irregular linear objects, which are easily affected by surface vegetation

Author Manuscript

and shadow, resulting in discontinuous phenomena in remote sensing images when visually interpreted. In contrast, both ENVINet5 and ENVINet5-OBIC generally produced satisfactory ground fissure extraction results with minimal noise and outlines that are remarkably aligned with the ground truth data. However, ENVINet5 produced local discontinuity of linear ground objects blurred by vegetation cover or shadow (Figure 6: blue rectangles), even though it aligned with the visually interpretation. This error was caused by spectral feature classification based on a single pixel. Nevertheless, by leveraging OBIC technique's attribute assessment between neighboring pixels, ENVINet5-OBIC overcomes this shortcoming. Extracted ground fissures were accurately outlined and parts of ground fissures that were covered by vegetation or shadows were correctly identified. ENVINet5-OBIC results demonstrated good continuity and were in accord with the ground truth data.

Author Manuscript

Author Manuscript

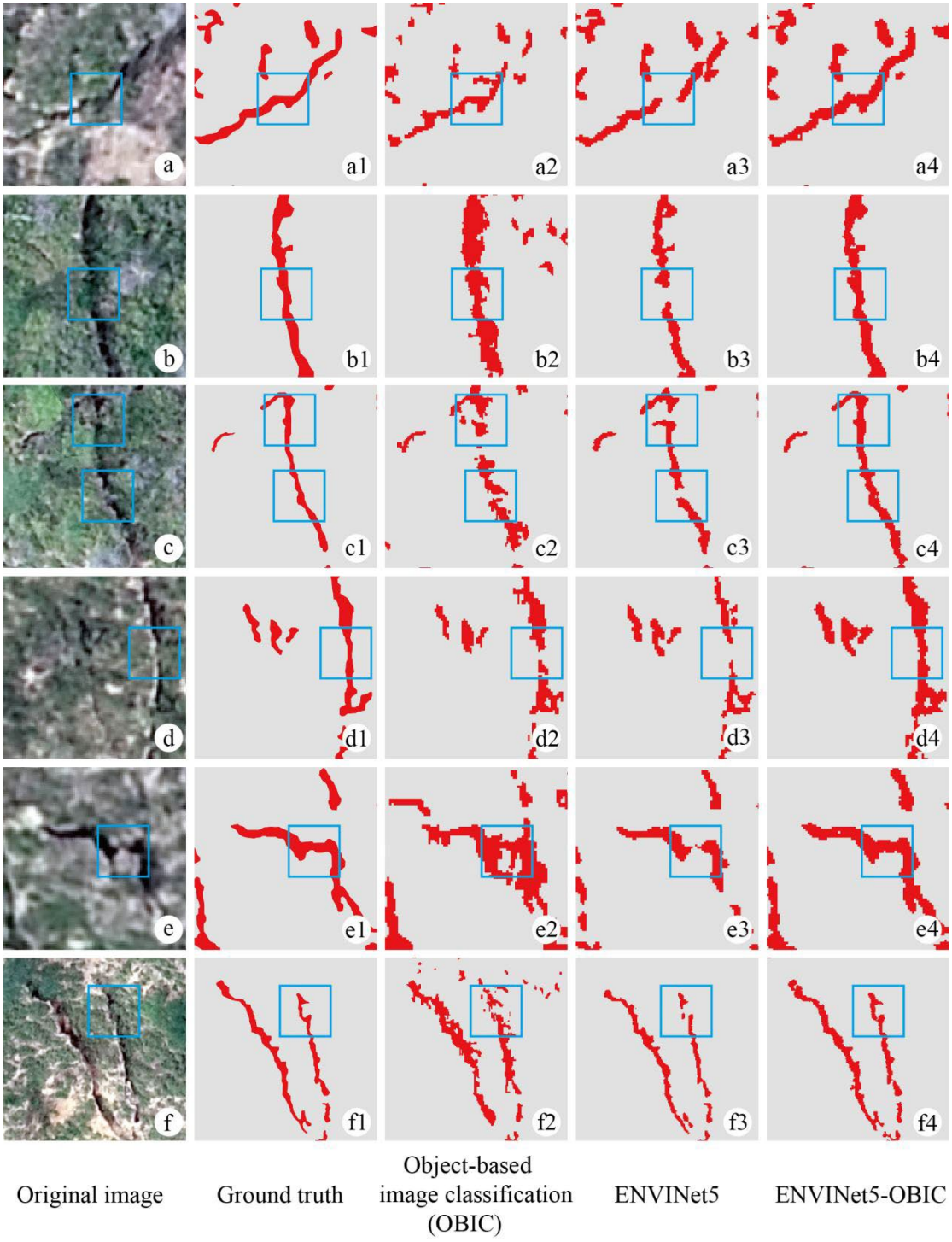


FIGURE 6 Ground fissures extraction results using VS. (a)-(f) Representative partial samples of ground fissures: blue rectangles represent the display of local extraction effects using OBIC, ENVINet5, and ENVINet5-OBIC methods.

The performance evaluation of the three methods using the VS was

quantitatively assessed by confusion matrix and its derived assessment indices (Figure 7). ENVINet5-OBIC produced higher TN and TP and lower FP and FN, indicating that its extraction results had fewer misclassifications and omissions (Figure 7a); TN and TP accounted for 98.7% when using ENVINet5-OBIC, which is 3.0% higher than using OBIC and 0.1% higher than using ENVINet5; FP and FN accounted for 1.3% when using ENVINet5-OBIC, which is 3.0% lower than using OBIC and 0.1% lower than using ENVINet5. Moreover, ENVINet5-OBIC reached an OA of 0.988, KC of 0.826, recall of 0.952, F1-score of 0.832, and MIoU of 0.850, which were 0.031, 0.281, 0.144, 0.288, and 0.185 higher than for OBIC, and 0.002, 0.051, 0.157, 0.047, and 0.034 higher than for ENVINet5 (Figure 7b). All assessment indices demonstrated better performance and superiority of ENVINet5-OBIC in ground fissure extraction.

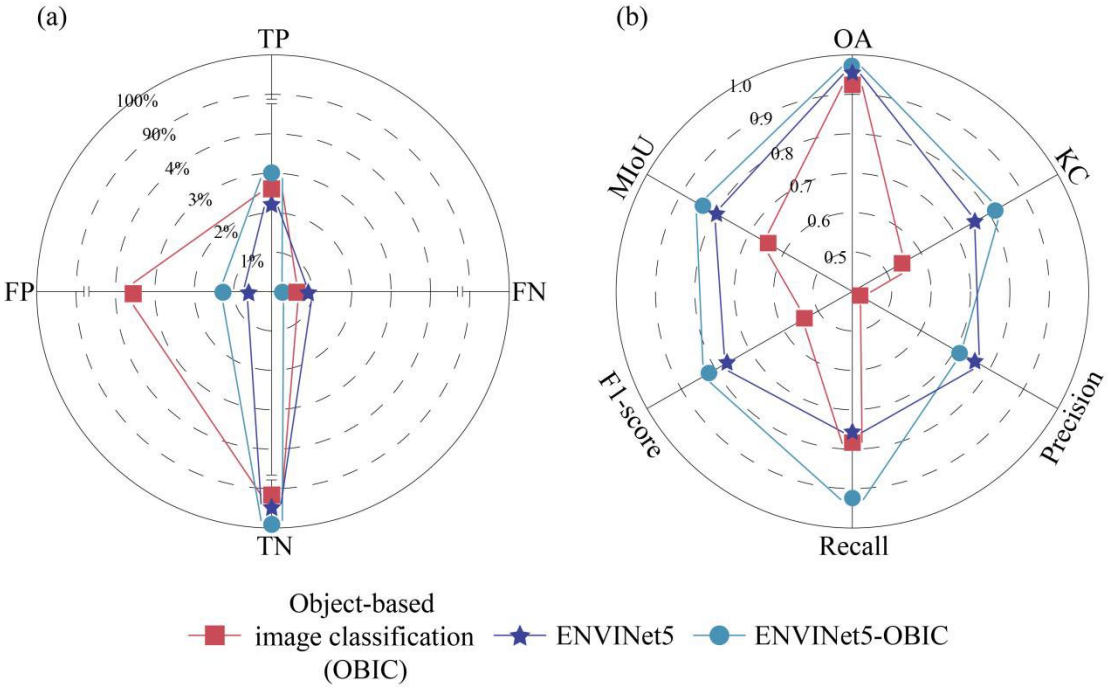


FIGURE 7 Performance of different ground fissures extraction approaches using VS. (a) Indices proportion of the confusion matrix. (b) Accuracy assessment of OBIC, ENVINet5, and ENVINet5-OBIC methods.

Author Manuscript

Author Manuscript

4.3. Error analysis of models

To further verify the superiority of the proposed method, CE and OE were calculated for both TS and VS, alongside losses for ENVINet5 and ENVINet5-OBIC (Figures 8 and 9). Using TS, ENVINet5-OBIC achieved a CE of 0.196 and OE of 0.062, which is significantly smaller compared to those using OBIC and ENVINet5 (Figure 8a). Using VS, CE of ENVINet5-OBIC was 0.261, which is 0.036 larger than that using ENVINet5. At the same time, OE of ENVINet5-OBIC was 0.048, which is 0.157 smaller than using ENVINet5 and 0.144 smaller than using OBIC (Figure 8b). Furthermore, using TS, ENVINet5-OBIC attained a loss of 0.053 when the Loss function stabilized, which is 0.005 smaller than using ENVINet5 (Figure 9a). When using VS, the loss of ENVINet5-OBIC settles at a point that is 0.0024 lower and reflects stronger robustness compared to using ENVINet5 (Figure 9b). ENVINet5-OBIC demonstrated a better performance in extracting ground fissures than ENVINet5 and OBIC.

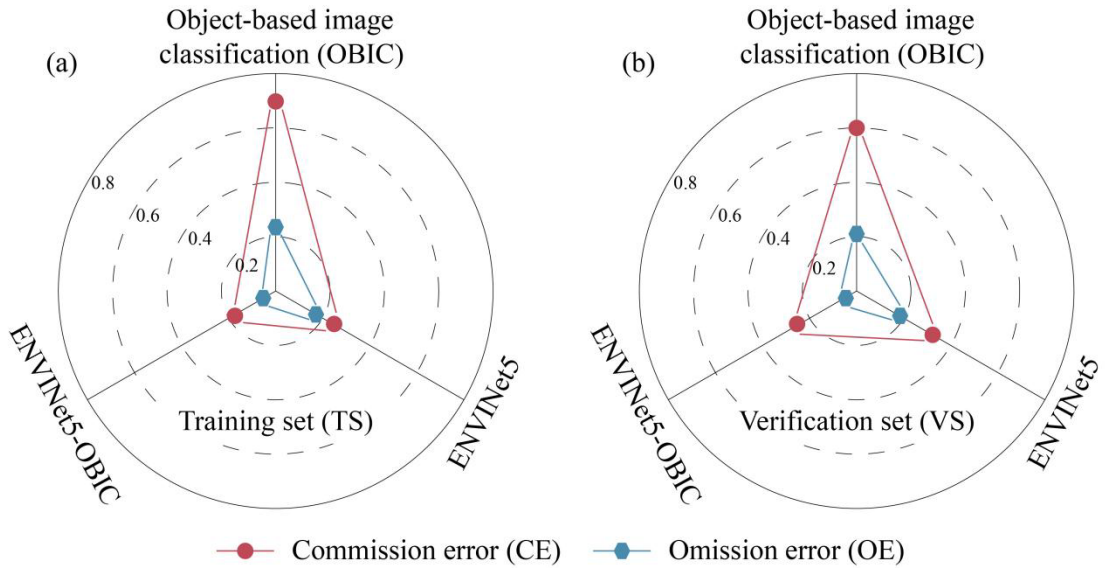


FIGURE 8 CE and OE analyses for three different analysis methods using (a) TS, and (b) VS.

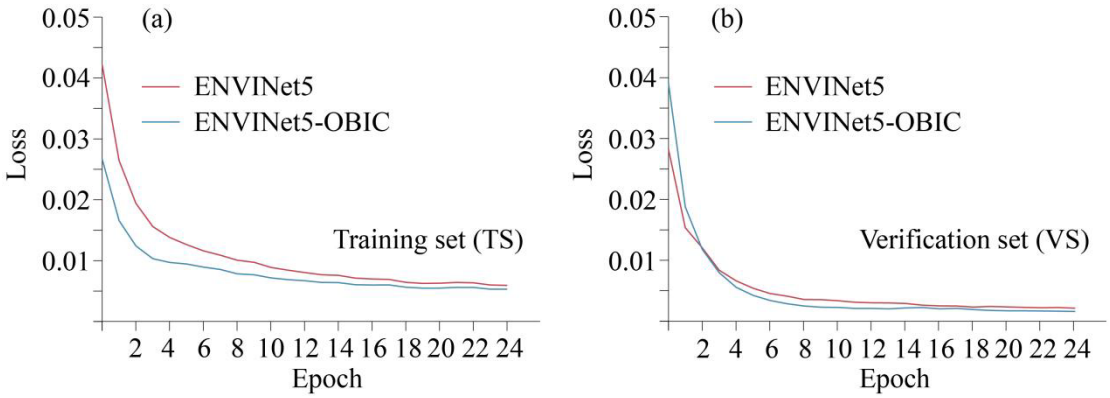


FIGURE 9 Loss function of deep learning models using (a) TS, and (b) VS.

4.4. Ground fissure extraction in representative field sites

To further verify the applicability of ENVINet5-OBIC, six representative field sites with a high number of ground fissures were selected, and OBIC, ENVINet5, and ENVINet5-OBIC were used in extracting ground fissures (Figure 10). Site 1 is located on the slope; Site 2 and Site 3 are found in a relatively gentle area with sparse vegetation cover and shallow, slender ground fissures; Site 4 sits above the landslide mass, where the ground fissures were caused by the displacement of the surface deformation before the landslide; Site 5 and Site 6 are positioned on the ridge.

OBIC generated a significant amount of noise and resulted in many misclassifications and omissions. While ENVINet5 resulted in fewer misclassifications, omissions occurred, particularly at ground fissures covered by vegetation and shadow, resulting in a lack of continuity. In contrast, ENVINet5-OBIC demonstrated minimal misclassifications and omissions. The extracted ground fissures maintained satisfactory continuity, closely resembling the ground truth. ENVINet5-OBIC can effectively suppress noise, and it can not only accurately identify and extract the outline of ground fissures, but also identify and extract the parts of ground fissures that are covered by vegetation and shadow based on the linear

Author Manuscript

characteristics of the ground fissures. ENVINet5-OBIC is feasible to accurately extract ground fissures.

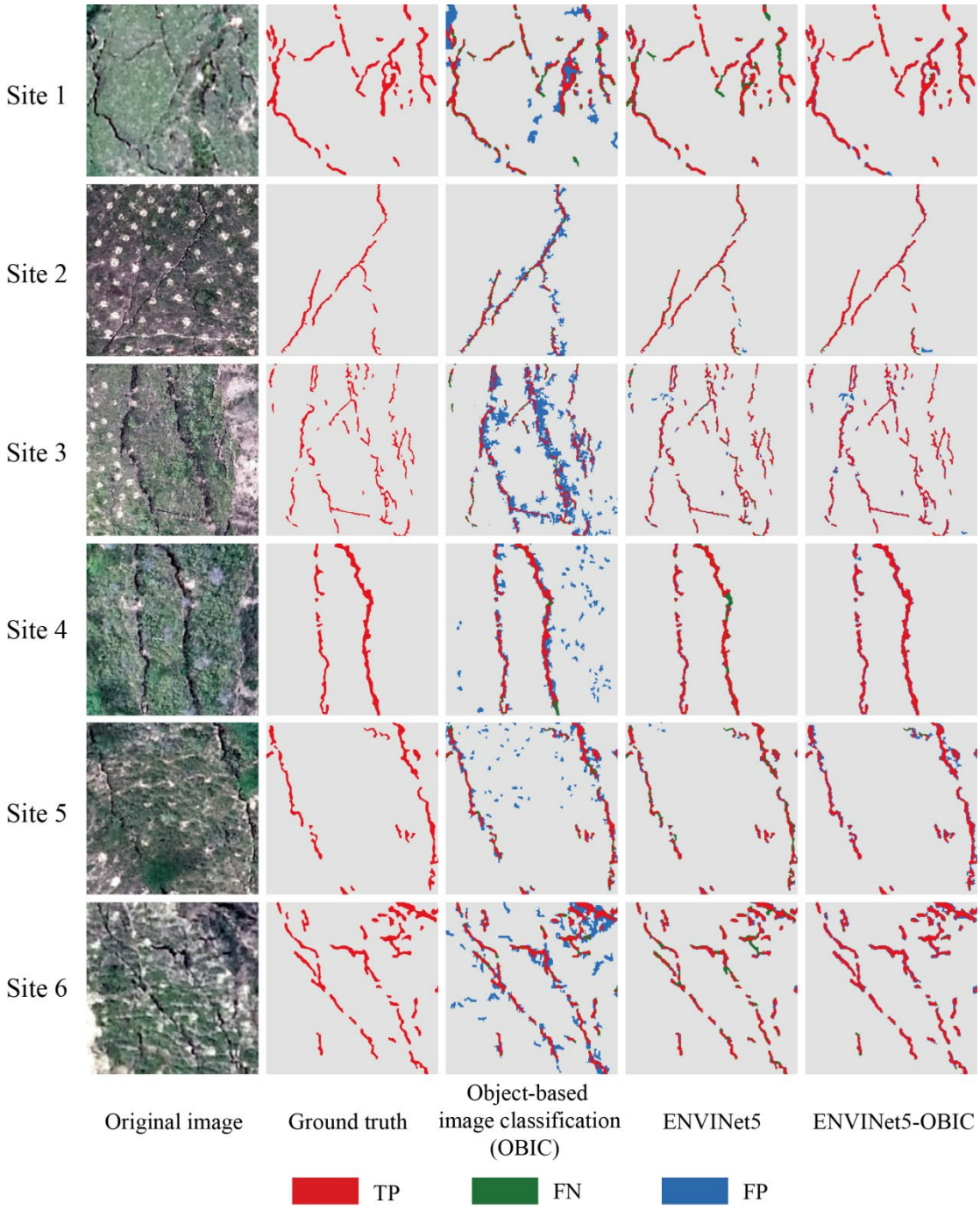


FIGURE 10 Ground fissures extracted results using three different methods in six representative field sites.

Receiver operating characteristics (ROC) can be used to assess performance in

Author Manuscript

Author Manuscript

extracting ground fissure. Previous studies suggested a technique involving multiple buffering of extracted linear datasets followed by overlaying with ground truth datasets to gauge the accuracy of linear object extraction (Tveite & Langaas, 1999). In this study, a total of ten buffer operations were performed using the center distance between two adjacent pixels as the step length. The different buffers were used for the overlay analysis, and the true positive rate (TPR) and the false positive rate (FPR) were repeatedly calculated (Figure 11). For the six sites, TPR using ENVINet5-OBIC was 89.6%, 89.6%, 91.3%, 93.3%, 92.3%, and 89.3%, while FPR was 3.2%, 6.2%, 5.9%, 8.2%, 10.2%, and 8.5%. ENVINet5-OBIC produced a higher TPR and lower FPR than ENVINet5 or OBIC.

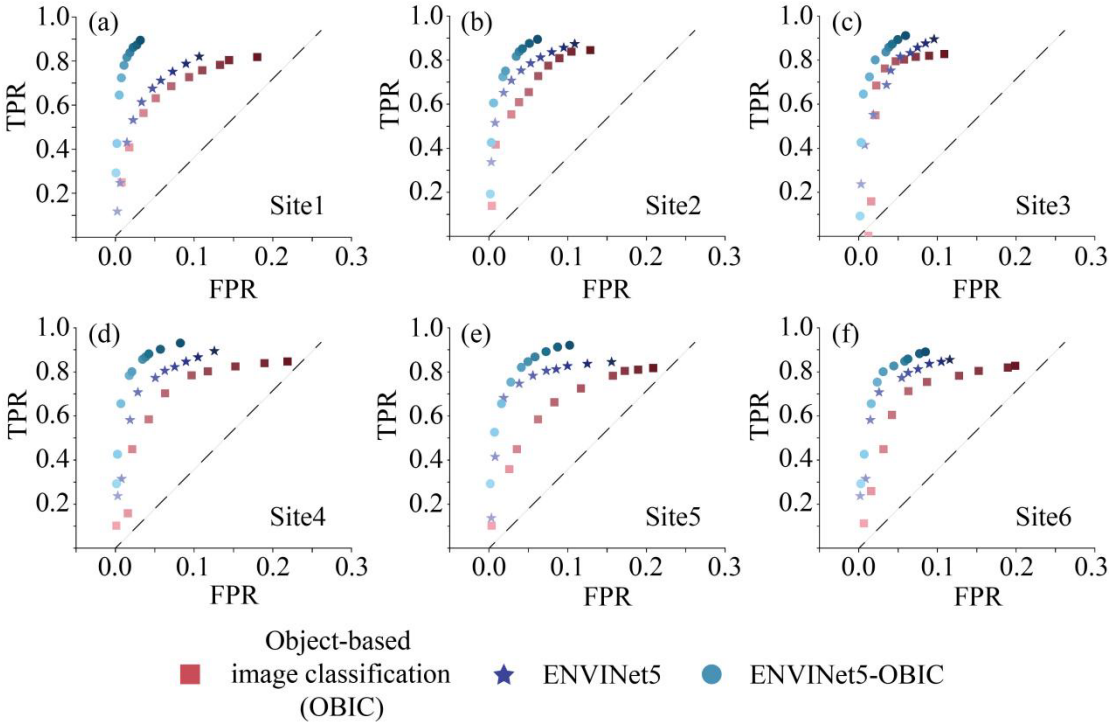


FIGURE 11 ROC plots for three different methods of ground fissure extraction in six representative field sites.

Finally, ENVINet5-OBIC was evaluated by comparing the extracted ground fissure areas with the ground truth data (Figure 12). Using all three extraction

methods, the coefficient of determination R^2 was >0.9 and RMSE was <1, documenting a generally strong correlation between the extracted ground fissures areas and the ground truth data. However, the correlation was the strongest when using ENVINet5-OBIC: R^2 was 0.987, which was 0.002 higher for ENVINet5 and 0.065 higher than for OBIC; RMSE was 0.271 and lower by 0.057 compared to ENVINet5 and by 0.523 compared to OBIC. ENVINet5-OBIC achieved the most accurate extraction results when compared to the ground truth data.

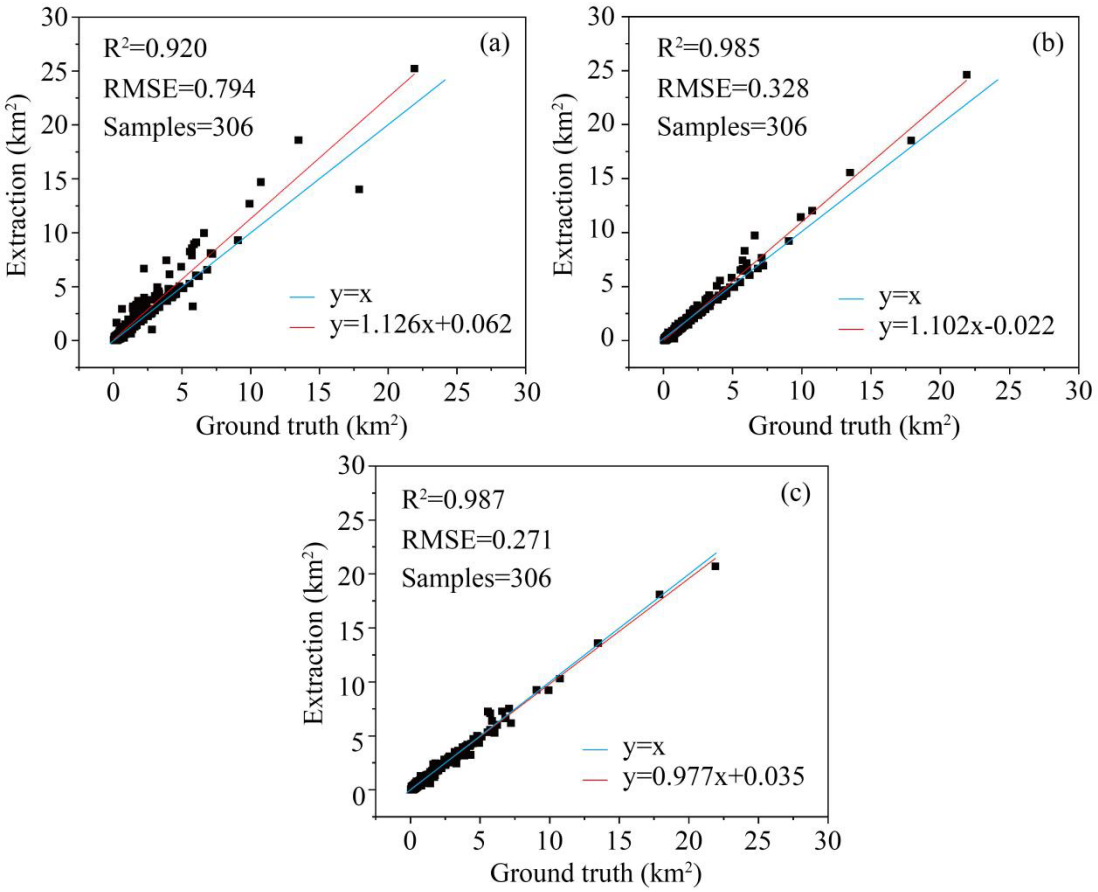


FIGURE 12 Comparison of extracted ground fissure areas with the ground truth data using three different extraction methods: (a) OBIC, (b) ENVINet5, (c) ENVINet5-OBIC

4.5. Comparison with other deep learning models

To further verify the overall good performance of the proposed ENINet5-OBIC

Author Manuscript

method in ground fissure extraction, it was compared to U-Net and PSPNet by combining them with OBIC to create U-Net-OBIC and PSPNet-OBIC. Figure 13 shows the ground fissure extraction results obtained by using different deep learning models. The extraction results using U-Net and PSPNet models were not satisfactory owing to many misclassifications and omissions, insufficient continuity and significant deviation from the ground truth. In contrast, U-Net-OBIC and PSPNet-OBIC effectively identified objects with weak feature information, and the continuity of the ground fissures improved. However, more misclassifications and omissions existed when compared to ENVINet5-OBIC.

The performance of different deep learning models was quantitatively assessed by accuracy assessment and error analysis (Figure 14). The accuracy assessment showed an OA of 0.989 for ENVINet5-OBIC, which was higher than that for PSPNet (by 0.023), PSPNet-OBIC (by 0.021), U-Net (by 0.002), and U-Net-OBIC (by 0.016). The KC of ENVINet5-OBIC reached 0.826, which was 0.216, 0.111, 0.134, and 0.041 higher than PSPNet, PSPNet-OBIC, U-Net, and U-Net-OBIC, respectively. In addition, Recall, F1-score, and MIoU of ENVINet5-OBIC were all higher than those of the comparison methods, reaching 0.952, 0.832, and 0.850, respectively. CE of ENVINet5-OBIC was 0.228, which was 0.256, 0.194, 0.125, and 0.012 smaller than that of PSPNet, PSPNet-OBIC, U-Net, and U-Net-OBIC, respectively. OE of ENVINet5-OBIC was 0.02, it is 0.181, 0.158, 0.232, and 0.137 smaller than PSPNet, PSPNet-OBIC, U-Net, and U-Net-OBIC, respectively. This performance assessment further proved that ENVINet5-OBIC obtained the best results in ground fissure extraction.

Author Manuscript

Author Manuscript

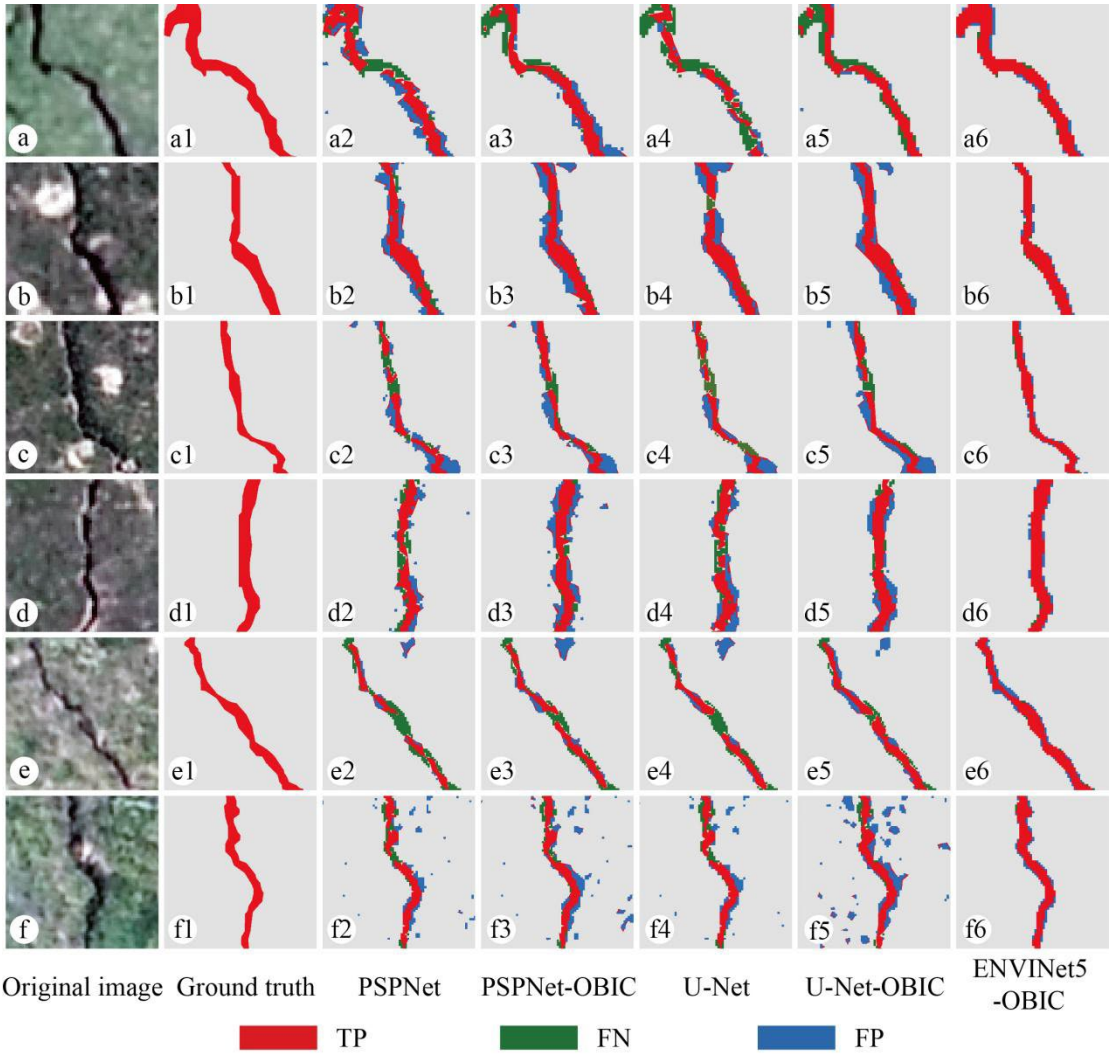


FIGURE 13 Ground fissures extracted results using different deep learning models.

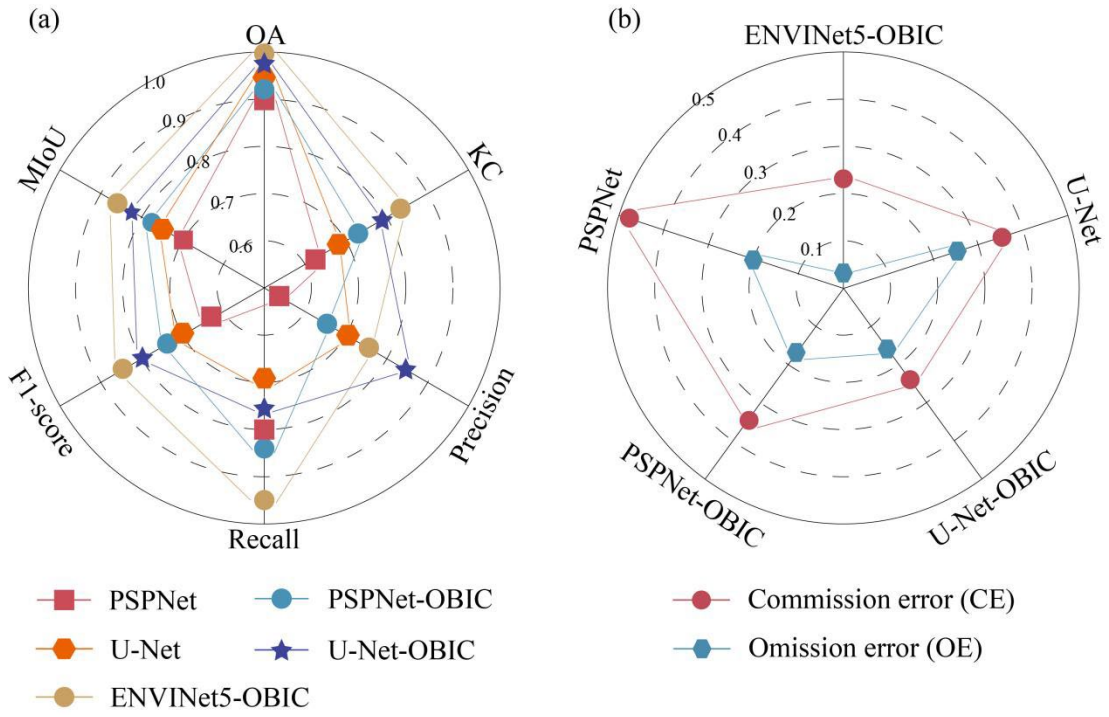


FIGURE 14 Performance of different deep learning models in ground fissures extraction. (a) Accuracy assessment. (b) CE and OE analyses.

5. Discussion

Ground fissures, arising from intense coal mining, represent a significant geological hazard. Developing precise and automated techniques for ground fissure extraction holds paramount importance. High-resolution UAV images can fully display the distribution characteristics of ground fissures and effectively extract objects information at the centimeter level. In this study, an ENVINet5-OBIC method is proposed for extracting ground fissures automatically and accurately, and it was compared to OBIC and pixel-based ENVINet5.

5.1. Interpretation of the extraction methods for ground fissures

Surfaces in coal mining landscapes are complex, but high-resolution UAV images contain abundant information about ground objects. The Matched Filter with First-order Derivative of Gaussian (MF-FDOG) algorithm combined with UAV

Author Manuscript

Author Manuscript

images has been used to extract surface fissures (Stumpf et al., 2013). However, when adjusting the range of values between two response images generated by filtering operation, MF-FDOG's sensitivity correction parameters have the disadvantage of weak universality, and using parameter empirical values has limitations. While an improved MF-FDOG algorithm achieved good results in extracting small fissures from loess areas (Jia et al., 2021), it was not feasible for detecting nonlinear distribution of fissures. Another approach combined the multiscale Hessian-based enhancement filter, single threshold operation, and incomplete path to extract ground fissures, but this threshold segmentation method is extremely sensitive to noise, and it is not obvious to the segmentation of objects with insignificant gray difference and overlapping gray values (Yang et al., 2022). Fu et al. (2023) proposed a ground fissure extraction method that combines geometric shape and optical features. A morphological method was used to de-noise the binary image, eliminating the object and noise of incorrect extraction. While this method of denoising was suitable for images with large object size and without many details, the morphology of ground fissures in mining areas is complex and diverse, and it is easy to remove small ground fissures as noise points, which leads to the reduction in extraction accuracy.

Machine learning models such as Support Vector Machine (SVM), K Nearest Neighbor (KNN), Random Forest (RF), Naive Bayes (NB), and Maximum Likelihood (ML) have been used to extract ground fissures in coal mining regions (Zhang et al., 2020; Li 2021; Yang et al., 2022; Hao et al., 2022). While their extraction speed and accuracy are greatly improved compared with traditional methods, these models rely largely on manually extracted features (Fan et al., 2018) and in a wide range of relatively complex ground object types. They produce many omissions and commissions, which cannot meet accuracy requirements. Deep learning models such

as DeepLabv3+ (Yuan et al., 2023), FCN (Alipour et al., 2019), and U-Net (Lau et al., 2020) rely on single-scale feature inputs and have been used to identify fissures in coal tunnels and concrete facilities. The Multi-scale Feature Pyramids and Attention Network model (MFPA-Net), relies on multi-scale feature information and is proposed to achieve more detailed ground fissure extraction in coal mining regions (Jiang et al., 2022). However, these deep learning models mainly take the pixels of high-resolution images as the basic unit and ignore the spatial relations and semantic information between adjacent pixels, which easily results in adjacent pixels of the same object being divided into different categories due to spectral differences, or adjacent pixels of different objects being divided into the same category due to spectral similarities.

ENVINet5-OBIC performs multi-scale segmentation of imagery and selects ground fissure samples based on homogeneous objects. ENVINet5-OBIC not only treats homogeneous objects as the basic units by fully integrating attribute associations among neighboring pixels, but also has the capacity to elevate low-level (spectral) features to high-level (semantic) features (Ammour et al., 2017; Andres et al., 2018; Kaur & Singh, 2022). This study has confirmed that ENVINet5-OBIC is superior to OBIC and ENVINet5 in extracting ground fissures. ENVINet5-OBIC not only achieves higher extraction accuracy, but also identifies parts of ground fissures covered by vegetation or shadows, and the extraction results have better continuity. The feature description of OBIC is designed based on low-level features, therefore, it is difficult to capture high-level semantic features and complex content, resulting in low learning efficiency (Lu et al., 2020; Ghorbanzadeh et al., 2022) and many false positive samples in the classification (Figures 6). Furthermore, OBIC relies on expert knowledge to obtain the best segmentation parameters and, thereby, has poor

Author Manuscript

Author Manuscript

generalization performance and robustness (Majd et al., 2019). The main difference between ENVINet5 and ENVINet5-OBIC is the label raster used to build models. The former selects ground fissure samples based on pixels, which only considers the spectral characteristics of a single pixel and ignores the attribute correlation between adjacent pixels. At the same time, this approach will also cause redundancy of spatial data and resource wastage, resulting in certain omissions and misclassification (Goetz et al., 2015). In addition, the comparison of ground fissure extraction results using ENVINet5-OBIC with PSPNet and U-Net models further proves the superiority of ENVINet5-OBIC.

5.2. Data quality control and future work

Ground fissures in coal mining regions show irregular linear distribution at the surface and are of relatively small widths ranging from a few centimeters to a few meters. To ensure accurate extraction of ground fissures in coal mining areas, a high quality of the collected UAV imagery is crucial. Enough GCPs and checkpoints must be set up for aerial photography as they help define the boundaries of the site, which can effectively improve the accuracy of the image. Surface vegetation has a certain impact on object extraction. Although airborne LiDAR drones can penetrate vegetation, they have a higher cost and are susceptible to bad weather. At present, UAV photogrammetry is still mainly used to generate optical remote sensing images (Jia et al., 2021; Yang et al., 2022; Jiang et al., 2022). To ensure a successful extraction of all ground fissures, weather conditions must be monitored prior to UAV operations to avoid restriction with image quality caused by clouds, fog, and common dust in the Loess Plateau region. Furthermore, vegetation enters the wilting period in the late autumn season, and a UAV field survey at this time can effectively reduce the disturbance from surface vegetation.

The proposed ENVINet5-OBIC approach can effectively extract parts of the ground fissures that are covered by vegetation or shadows, which enhances the continuity of the results. However, ENVINet5-OBIC only extracts the location and area information of ground fissures, but it cannot automatically obtain fissure types or other information. To address these issues and offer more comprehensive services for environmental monitoring in mining areas, further research needs to be conducted.

6. Conclusion

In view of inadequate accuracy of pixel-based techniques in extracting ground fissures within coal mining regions and the issue of local discontinuity caused by vegetation and shadow coverage, this study introduces a novel approach to improve extraction results. It uses high-resolution UAV imagery and integrates OBIC with deep learning methods to construct our ENVINet5-OBIC method for the extraction of ground fissures. OBIC and pixel-based ENVINet5 were used to verify the feasibility of the proposed method. ENVINet5-OBIC effectively combines the strengths of both OBIC and ENVINet5 methods. By comprehensively learning and analyzing homogenous objects within the image, the method achieves a high level of continuity in the extracted ground fissures. Clearly, ENVINet5-OBIC demonstrates superior performance compared to OBIC and ENVINet5, which is expressed in higher accuracy, reduced error, and ground fissure area estimations that closely align with ground truth data. This study provides a new method for the automatic and accurate extraction of ground fissures in mining region, which is helpful to further improve the efficiency of environmental monitoring.

Author Manuscript

Author Manuscript

References

Ammour, N., Alhichri, H., Bazi, Y., Benjdira, B., Alajlan, N. & Zuair, M. (2017) Deep learning approach for car detection in UAV imagery. *Remote Sensing*, 9, 312. https://doi.org/10.3390/rs9040312

Andres, M., Philipp, L. & Cyrill, S. (2018) Real-Time Semantic Segmentation of Crop and Weed for Precision Agriculture Robots Leveraging Background Knowledge in CNNs. *2018 IEEE International Conference on Robotics and Automation (ICRA), Brisbane, QLD, Australia*, pp 2229-2235. https://doi.org/10.1109/ICRA.2018.8460962

Alipour, M., Harris, D.K. & Miller, G.R. (2019) Robust Pixel-Level Crack Detection Using Deep Fully Convolutional Neural Networks. *J. Comput. Civil Eng*, 33, 04019040. https://doi.org/10.1061/(ASCE)CP.1943-5487.0000854

Blaschke, T., Hay, G.J., Kelly, M., Lang, S., Hofmann, P., Addink, E., Feitosa, R.Q., Vander Meer F, Van der Werff H, Van Coillie F (2014) Geographic object-based image analysis-towards a new paradigm. *ISPRS J Photogramm Remote Sens*, 87:180-191. https://doi.org/10.1016/j.isprsjprs.2013.09.014

Bhowmick, S., Nagarajaiah, S. & Veeraraghavan, A. (2020) Vision and Deep Learning-Based Algorithms to Detect and Quantify Cracks on Concrete Surfaces from UAV Videos. *Sensors*, 20(21), 6299. https://doi.org/10.3390/s20216299

Cheng, G., Guo, L., Zhao, T., Han, J., Li, H. & Fang, J. (2013) Automatic landslide detection from remote-sensing imagery using a scene classification method based on BoVW and pLSA. *International Journal of Remote Sensing*, 34, 45–59. https://doi.org/10.1080/01431161.2012.705443

Chan, T.H., Jia, K., Gao, S., Lu, J., Zeng, Z. & Ma, Y. (2015) PCANet: a simple deep learning baseline for image classification? *IEEE Transactions on Image*

Author Manuscript

Processing, 24(12), 5017–5032. https://doi.org/10.1109/TIP.2015.2475625

Chen, F., Yu, B. & Li, B. (2018) A practical trial of landslide detection from single-temporal Landsat8 images using contour-based proposals and random forest: a case study of national Nepal. *Landslides*, 15, 453–464. https://doi.org/10.1007/s10346-017-0884-x

Carlà, T., Intrieri, E., Raspini, F., Bardi, F., Farina, P., Ferretti, A., Colombo, D., Novali, F. & Casagli, N. (2019) Perspectives on the prediction of catastrophic slope failures from satellite InSAR. *Sci Rep*, 9(1), 14137. https://doi.org/10.1038/s41598-019-50792-y

Chen, B., Li, Z., Yu, C., Fairbairn, D., Kang, J., Hu, J. & Liang, L. (2020) Three-dimensional time-varying large surface displacements in coal exploiting areas revealed through integration of SAR pixel offset measurements and mining subsidence model. *Remote Sens. Environ*, 240, 111663. https://doi.org/10.1016/j.rse.2020.111663

Daniel, H., Petra, F., Francesco, A., Francesca, C., Nicola, C. & Lang, S. (2012) A semi-automated object-based approach for landslide detection validated by persistent scatterer interferometry measures and landslide inventories. *Remote Sensing*, 4(5), 1310-1336. https://doi.org/10.3390/rs4051310

Drăguţ L, Csillik O, Eisank C, et al. (2014) Automated parameterisation for multi-scale image segmentation on multiple layers. *ISPRS Journal of Photogrammetry and Remote Sensing*, 88, 119-127. https://doi.org/10.1016/j.isprsjprs.2013.11.018

Du, B., Zhao, Z., Hu, X., Wu, G., Han, L., Sun, L. & Gao, Q. (2021) Landslide susceptibility prediction based on image semantic segmentation. *Computers & Geosciences*, 155, 104860. https://doi.org/10.1016/j.cageo.2021.104860

Author Manuscript

Eeckhaut, M., Kerle, N., Poesen, J. & Hervas, J. (2012) Object-oriented identification of forested landslides with derivatives of single pulse LIDAR data. *Geomorphology*, 173–174, 30-42. https://doi.org/10.1016/j.geomorph.2012.05.024

Fawcett, T. (2006) An introduction to ROC analysis. *Pattern Recognition Letters*, 27, 861-874. https://doi.org/10.1016/j.patrec.2005.10.010

Fan, Z., Wu, Y., Lu, J. & Li, W. (2018) Automatic pavement crack detection based on structured prediction with the convolutional neural network. *arXiv e-prints*,1802.02208. https://doi.org/10.48550/arXiv.1802.02208

Fei, Y., Wang, K.C.P., Zhang, A., Chen, C., Li, J.Q., Liu, Y., Yang, G. & Li, B. (2020) Pixel-Level Cracking Detection on 3D Asphalt Pavement Images Through Deep-Learning-Based CrackNet-V. *IEEE Transactions on Intelligent Transportation Systems*, 21, 273–284. https://doi.org/10.1109/TITS.2019.2891167

Fu, Y., Shang, J., Hu, Z., Li, P., Yang, K., Chen, C., Guo, J. & Yuan, D. (2021) Ground fracture development and surface fracture evolution in N00 method shallowly buried thick coal seam mining in an arid windy and sandy area: A case study of the Ningtiaota Mine (China). *Energies*, 14(22), 7712. https://doi.org/10.3390/en14227712

Goetz, J.N., Brenning, A., Petschko, H. & Leopold, P. (2015) Evaluating machine learning and statistical prediction techniques for landslide susceptibility modeling. *Computers & Geosciences*, 81, 1-11. https://doi.org/10.1016/j.cageo.2015.04.007

Ghorbanzadeh, O., Shahabi, H., Crivellari, A., Homayouni, S., Blaschke, T. & Ghamisi, P. (2022) Landslide detection using deep learning and object-based

Author Manuscript

image analysis. *Landslides*, 19, 929-939. https://doi.org/10.1007/s10346-021-01843-x

Hu, Z.Q., Wang, X.J. & He, A.M. (2014) Distribution characteristic and development rules of ground fissures due to coal mining in windy and sandy region. *J. China Coal Soc*, 39(1), 11-18 (in Chinese). https://doi.org/10.13225/j.cnki.jccs.2013.1289

Hölbling, D., Friedl, B. & Eisank, C. (2019) Correction to: An object-based approach for semi-automated landslide change detection and attribution of changes to landslide classes in northern Taiwan. *Earth Sci. Inform*, 12, 275. https://doi.org/10.1007/s12145-018-00375-8

He, T.T., Xiao, W., Zhao, Y.L., Deng, X.Y. & Hu, Z.Q. (2020) Identification of waterlogging in Eastern China induced by mining subsidence: a case study of Google Earth Engine time-series analysis applied to the Huainan coal field. *Remote Sens. Environ*, 242, 111742. https://doi.org/10.1016/j.rse.2020.111742

He, Q., Wang, M. & Liu, K. (2021) Rapidly assessing earthquake-induced landslide susceptibility on a global scale using random forest. *Geomorphology*, 391, 107889. https://doi.org/10.1016/j.geomorph.2021.107889

Hao, M., Lin, H.J. & Gao, Y.Y. (2022) Ground fissure extraction method based on improved active contour model for UAV images in mining areas. *Journal of Geo-information Science*, 24 (12), 2448-2457. (In Chinese)

Janardhanan, P.S. (2020) Project repositories for machine learning with tensorflow. *Procedia Computer Science*, 171, 188-196. https://doi.org/10.1016/j.procs.2020.04.020

Ji, A.K., Xue, X.L., Wang, Y., Luo, X.W. & Xue, W.R. (2020) An integrated approach to automatic pixel-level crack detection and quantification of asphalt pavement.

Author Manuscript

Automation in Construction, 114, 103176. https://doi.org/10.1016/j.autcon.2020.103176

Jia, H., Wei, B., Liu, G., Zhang, R., Yu, B. & Wu, S. (2021) A Semi-Automatic Method for Extracting Small Ground Fissures from Loess Areas Using Unmanned Aerial Vehicle Images. *Remote Sens*, 13(9), 1784. https://doi.org/10.3390/rs13091784

Jiang, X., Mao, S.J., Li, M., Liu, H., Zhang, H.Y., Fang, S.W., Yuan, M.Z. & Zhang, C. (2022) MFPA-Net: An efficient deep learning network for automatic ground fissures extraction in UAV images of the coal mining area. *International Journal of Applied Earth Observation and Geoinformation*, 114, 103039. https://doi.org/10.1016/j.jag.2022.103039

Kong, J.L., Xian, T., Yang, J., Chen, L. & Yang, X.T. (2016) Monitoring soil moisture in a coal mining area with multi-phase LANDSAT images. *ISPRS International Archives of the Photogrammetry, Remote Sensing and Spatial Information Sciences*, XLI-B7, 537-542. https://doi.org/10.5194/isprs-archives-XLI-B7-537-2016

Kaur, R. & Singh, S. (2022) A comprehensive review of object detection with deep learning. *Digital Signal Processing*, 132, 103812. https://doi.org/10.1016/j.dsp.2022.103812

Kheradmandi, N. & Mehranfar, V. (2022) A critical review and comparative study on image segmentation-based techniques for pavement crack detection. *Constr. Build. Mater*, 321, 126-162. https://doi.org/10.1016/j.conbuildmat.2021.126162

Landis, J.R. & Koch, G.G. (1977) The measurement of observer agreement for categorical data. *Biometrics*, 33, 159–174. https://doi.org/10.2307/2529310

Lu, P., Stumpf, A., Kerle, N. & Casagli, N. (2011) Object-oriented change detection

Author Manuscript

for landslide rapid mapping. *IEEE Geosci. Remote Sens. Lett*, 8(4), 701–705. https://doi.org/10.1109/LGRS.2010.2101045

Li, L., Wu, K., Hu, Z., Xu, Y. & Zhou, D. (2017) Analysis of developmental features and causes of the ground cracks induced by oversized working face mining in an aeolian sand area. *Environ Earth Sci*, 76, 135. https://doi.org/10.1007/s12665-017-6452-9

Liu, H., Deng, K.Z., Zhu, X.J. & Jiang, C.L. (2019) Effects of mining speed on the developmental features of mining-induced ground fissures. *Bull Eng Geol Environ*, 78, 6297–6309. https://doi.org/10.1007/s10064-019-01532-z

Lau, S.L.H., Chong, E.K.P., Yang, X.u. & Wang, X. (2020) Automated pavement crack segmentation using u-net-based convolutional neural network. *IEEE Access*, 8, 114892–114899. https://doi.org/10.1109/ACCESS.2020.3003638

Lu, H., Ma, L., Fu, X., Liu, C., Wang, Z., Tang, M. & Li, N. (2020) Landslides information extraction using object-oriented image analysis paradigm based on deep learning and transfer learning. *Remote Sens*, 12(5), 752. http://dx.doi.org/10.3390/rs12050752

Li L K. (2021) Research on characteristics of surface cracks based on UAV image. Xi'an: Xi'an University of Science and Technology. (In Chinese)

Liu, Y., Qiu, H., Kamp, U., Wang, N., Wang, J., Huang, C. & Tang, B. (2024) Higher temperature sensitivity of retrogressive thaw slump activity in the Arctic compared to the Third Pole. *Science of the Total Environment*, 914, 170007. https://doi.org/10.1016/j.scitotenv.2024.170007

Martha, T.R., Kerle, N., Westen, C., Jetten, V. & Kumar, K.V. (2012) Object-oriented analysis of multi-temporal panchromatic images for creation of historical landslide inventories. *ISPRS Journal of Photogrammetry & Remote Sensing*, 67,

Author Manuscript

105–119. https://doi.org/10.1016/j.isprsjprs.2011.11.004

Malinowska, A.A. & Hejmanowski, R. (2016) The impact of deep underground coal mining on Earth fissure occurrence. *Acta Geodyn. Geomater*, 13(4), 321-330. https://doi.org/ 10.13168/AGG.2016.0014

Michoud, C., Baumann, V., Lauknes, T.R., Penna, I., Derron, M.H. & Jaboyedoff, M. (2016) Large slope deformations detection and monitoring along shores of the Potrerillos dam reservoir, Argentina, based on a small-baseline InSAR approach. *Landslides*, 13, 451-465. https://doi.org/10.1007/s10346-015-0583-4

Majd, R.D., Momeni, M. & Moallem, P. (2019) Transferable object-based framework based on deep convolutional neural networks for building extraction. *IEEEJ Sel Top Appl Earth Obs Remote Sens*, 12(8), 2627-2635. https://doi.org/10.1109/JSTARS.2019.2924582

Ma, S., Qiu, H., Yang, D., Wang, J., Zhu, Y., Tang, B., Sun, Kui. & Cao, M. (2023) Surface multi-hazard effect of underground coal mining. *Landslides*, 20, 39-52. https://doi.org/10.1007/s10346-022-01961-0

Nnolim, U.A. (2020) Automated crack segmentation via saturation channel thresholding, area classification and fusion of modified level set segmentation with canny edge detection. *Heliyon*, 6(12), e05748. https://doi.org/10.1016/j.heliyon.2020.e05748

Parker, R.N., Densmore, A.L., Rosser, N.J., De, M.M., Li, Y., Huang, R., Whadcoat, S. & Petley, D.N. (2011) Mass wasting triggered by the 2008 wenchuan earthquake is greater than orogenic growth. *Nature Geoscience*, 4, 449-452. https://doi.org/10.1038/ngeo1154

Perry, B.J., Guo, Y., Atadero, R. & Lindt, J.W. (2020) Streamlined bridge inspection system utilizing unmanned aerial vehicles (UAVs) and machine learning.

Author Manuscript

Measurement, 164, 108048. https://doi.org/10.1016/j.measurement.2020.108048

Pei, Y., Qiu, H., Yang, D., Liu, Z., Ma, S., Li, J., Cao, M. & Wufuer, W. (2023) Increasing landslide activity in the Taxkorgan River Basin (eastern Pamirs Plateau, China) driven by climate change. *CATENA*, 223, 106911. https://doi.org/10.1016/j.catena.2023.106911

Qu, F., Qiu, H., Sun, H. & Tang, M. (2021) Post-failure landslide change detection and analysis using optical satellite Sentinel-2 images. *Landslides*, 18, 447-455. https://doi.org/10.1007/s10346-020-01498-0

Qiu, H.J., Zhu, Y.R., Zhou, W.Q., Sun, H.S., He, J.Y. & Liu, Z.J. (2022) Influence of DEM resolution on landslide simulation performance based on the Scoops3D model. *Geomatics, Natural Hazards and Risk*, 13(1), 1663-1681. https://doi.org/10.1080/19475705.2022.2097451

Ronneberger, O., Fischer, P. & Brox, T. (2015) U-Net: Convolutional Networks for Biomedical Image Segmentation. *Springer International Publishing: Cham, Sitzerland*, pp 234–241. https://doi.org/10.48550/arXiv.1505.04597

Stumpf, A. & Kerle, N. (2011) Object-oriented mapping of landslides using random forests. *Remote Sensing of Environment*, 115(10), 2564-2577. https://doi.org/10.1016/j.rse.2011.05.013

Stumpf, A., Malet, J.P., Kerle, N., Niethamme, U. & Rothmund, S. (2013) Image-based mapping of surface fissures for the investigation of landslide dynamics. *Geomorphology*, 186, 12-27. https://doi.org/10.1016/j.geomorph.2012.12.010

Sujatha, C. & Selvathi, D. (2015) Connected component-based technique for automatic extraction of road centerline in high resolution satellite images. *EURASIP Journal on Image and Video Processing*, 8(2015).

Author Manuscript

https://doi.org/10.1186/s13640-015-0062-9

Tveite, H. & Langaas, S. (1999) An accuracy assessment method for geographical line data sets based on buffering. *International Journal of Geographical Information Science*, 13, 27–47. https://doi.org/10.1080/136588199241445

Tian, R., Sun, G., Liu, X. & Zheng, B. (2021) Sobel Edge Detection Based on Weighted Nuclear Norm Minimization Image Denoising. *Electronics*, 10, 655. https://doi.org/10.3390/electronics10060655

Wang, L., Qiu, H., Zhou, W., Zhu, Y., Liu, Z., Ma, S., Yang, D. & Tang, B. (2022) The post-failure spatiotemporal deformation of certain translational landslides may follow the pre-failure pattern. *Remote Sensing*, 14, 2333. https://doi.org/10.3390/rs14102333

Weibin, Kong., Jianzhao, Chen., Yubin, Song., Zhongqing, Fang., Xiaofang, Yang. & Hongyan, Zhang. (2023) "Sobel Edge Detection Algorithm with Adaptive Threshold based on Improved Genetic Algorithm for Image Processing". International Journal of Advanced Computer Science and Applications(IJACSA), 14(2). http://dx.doi.org/10.14569/IJACSA.2023.0140266

Yang, X., Wen, G., Dai, L., Sun, H. & Li, X. (2019) Ground subsidence and surface cracks evolution from shallow-buried close-distance multi-seam mining: A case study in Bulianta Coal Mine. *Rock Mech Rock Eng*, 52, 2835–2852. https://doi.org/10.1007/s00603-018-1726-4

Yu, B., Xu, C., Chen, F., Wang, N. & Wang, L. (2022) HADeenNet: A hierarchical-attention multi-scale deconvolution network for landslide detection. *International Journal of Applied Earth Observation and Geoinformation*, 111, 1569-8432. https://doi.org/10.1016/j.jag.2022.102853

Yang, K., Hu, Z., Liang, Y., Fu, Y., Yuan, D., Guo, J., Li, G. & Li, Y. (2022)

Author Manuscript

Automated Extraction of Ground Fissures Due to Coal Mining Subsidence Based on UAV Photogrammetry. *Remote Sens*, 14(5), 1071. https://doi.org/10.3390/rs14051071

Yang, D., Qiu, H., Ma, S., Liu, Z., Du, C., Zhu, Y. & Cao, M. (2022) Slow surface subsidence and its impact on shallow loess landslides in a coal mining area. *Catena*, 209, 105830. https://doi.org/10.1016/j.catena.2021.105830

Yang Q R, Hu Z Q, Han J Z, et al. (2022) Research on extraction method of ground fissures from UAV image mining in coal mine. *Coal Science and Technology*, 1-13. (In Chinese)

Ye, X., Zhu, H.H., Wang, J., Zhang, Q., Shi, B., Schenato, L. & Pasuto, A. (2022) Subsurface multi-physical monitoring of a reservoir landslide with the fiber-optic nerve system. *Geophysical Research Letters*, 49(11), e2022GL098211. https://doi.org/10.1029/2022GL098211

Yuan, Y.X., Zhang, N., Han, C.L. & Liang, D.X. (2023) Automated identification of fissure trace in mining roadway via deep learning. *Journal of Rock Mechanics and Geotechnical Engineering*, 15(8), 2039-2052. https://doi.org/10.1016/j.jrmge.2022.12.018

Yang, D.D., Qiu, H.J., Ye, B.F., Liu, Y., Zhang, J.J. & Zhu, Y.R. (2023) Distribution and Recurrence of Warming-induced Retrogressive Thaw Slumps on the Central Qinghai-Tibet Plateau. *Journal of Geophysical Research: Earth Surface*, 128(8), e2022JF007047. https://doi.org/10.1029/2022JF007047

Ye, B.F., Qiu, H.J., Tang, B.Z., Liu, Y., Liu, Z.J., Jiang, X.Y., Yang, D.D., Ullah, M., Zhu, Y.R. & Kamp, U. (2024) Creep deformation monitoring of landslides in a reservoir area. *Journal of Hydrology*, 632, 130905. https://doi.org/10.1016/j.jhydrol.2024.130905

Author Manuscript

Zhang, Y.D., Wu, L.N. & Wang, S.H. (2011) Magnetic resonance brain image classification by an improved artificial bee colony algorithm. *Progress In Electromagnetics Research*, 116, 65-79. https://doi.org/10.2528/PIER11031709

Zhao, H.J., Ma, F.S., Zhang, Y.M. & Guo, J. (2013) Monitoring and mechanisms of ground deformation and ground fissures induced by cut-and-fill mining in the Jinchuan Mine 2, China. *Environ Earth Sci*, 68(7), 1903-1911. https://doi.org/10.1007/s12665-012-1877-7

Zhang, L., Yang, F., Zhang, Y.D. & Zhu, Y.J. (2016) Road crack detection using deep convolutional neural network. *IEEE International Conference on Image Processing (ICIP), Phoenix, AZ, USA*, 3708-3712. https://doi.org/10.1109/ICIP.2016.7533052

Zhang, A., Wang, K.C.P., Fei, Y., Liu, Y., Tao, S., Chen, C. & Li, J.Q. (2018) Deep Learning-Based Fully Automated Pavement Crack Detection on 3D Asphalt Surfaces with an Improved Crack Net. *Journal of Computing in Civil Engineering*, 32(5), 04018041.1-04018041.14. https://doi.org/10.1061/(ASCE)CP.1943-5487.0000775

Zhang, L., Xu, W.C., Zhu, L.L., Yuan, X.Z. & Zhang, C. (2019) Study on pavement defect detection based on image processing utilizing UAV. *J. Phys. Conf. Ser*, 1168, 042011. https://doi.org/10.1088/1742-6596/1168/4/042011

Zhou, D.W., Wu, K., Bai, Z.H., Hu, Z.Q., Li, L., Xu, Y.K. & Diao, X.P. (2019) Formation and development mechanism of ground crack caused by coal mining: Effects of overlying key strata. *Bull. Eng. Geol. Environ*, 78, 1025-1044. https://doi.org/10.1007/s10064-017-1108-2

Zhang, F., Hu, Z., Fu, Y., Yang, K., Wu, Q. & Feng, Z. (2020) A New Identification Method for Surface Cracks from UAV Images Based on Machine Learning in

Author Manuscript

Coal Mining Areas. *Remote Sens*, 12, 1571. https://doi.org/10.3390/rs12101571

Zhang, P., Xu, C., Ma, S., Shao, X. & Wen, B. (2020) Automatic extraction of seismic landslides in large areas with complex environments based on deep learning: an example of the 2018 Iburi earthquake, Japan. *Remote Sens*, 12(23), 3992. https://doi.org/10.3390/rs12233992

Zollini, S., Alicandro, M., Dominici, D., Quaresima, R. & Giallonardo, M. (2020) UAV photogrammetry for concrete bridge inspection using object-based image analysis (OBIA). *Remote Sens*, 12(19), 3180. https://doi.org/10.3390/rs12193180

Zhao, Y., Sun, B.O., Liu, S., Zhang, C., He, X., Xu, D. & Tang, W. (2021) Identification of mining induced ground fissures using UAV and infrared thermal imager: Temperature variation and fissure evolution. *ISPRS J. Photogramm. Remote Sens*, 180, 45-64. https://doi.org/10.1016/j.isprsjprs.2021.08.005

Zhou, W.Q., Qiu, H.J., Wang, L.Y., Pei, Y.Q., Tang, B.Z., Ma, S.Y., Yang, D.D. & Cao, M.M. (2022) Combining rainfall-induced shallow landslides and subsequent debris flows for hazard chain prediction. *CATENA*, 213, 106199. https://doi.org/10.1016/j.catena.2022.106199

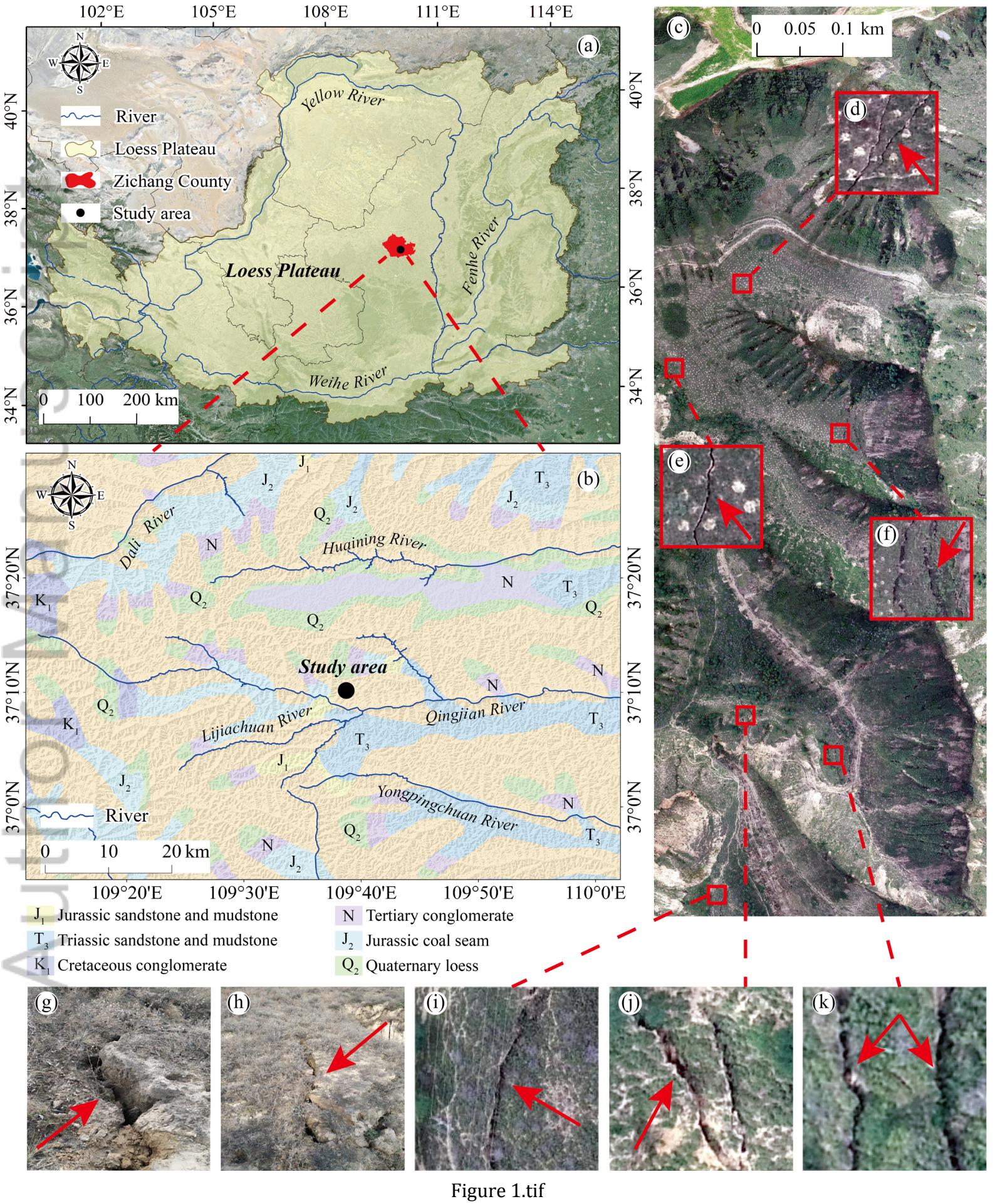

102°E
105°E
108°E
111°E
114°E
40°N
38°N
36°N
34°N
(a)
River
Loess Plateau
Zichang County
Study area
Yellow River
Fenhe River
Weihe River
Loess Plateau
0 100 200 km
(b)
Dali River
Huaining River
Qingjian River
Lijiachuan River
Yongpingchuan River
Study area
River
0 10 20 km
37°20'N
37°10'N
37°0'N
109°20'E
109°30'E
109°40'E
109°50'E
110°0'E
(c)
0 0.05 0.1 km
(d)
(e)
(f)
J1 Jurassic sandstone and mudstone
T3 Triassic sandstone and mudstone
K1 Cretaceous conglomerate
N Tertiary conglomerate
J2 Jurassic coal seam
Q2 Quaternary loess
(g)
(h)
(i)
(j)
(k)

Figure 1.tif

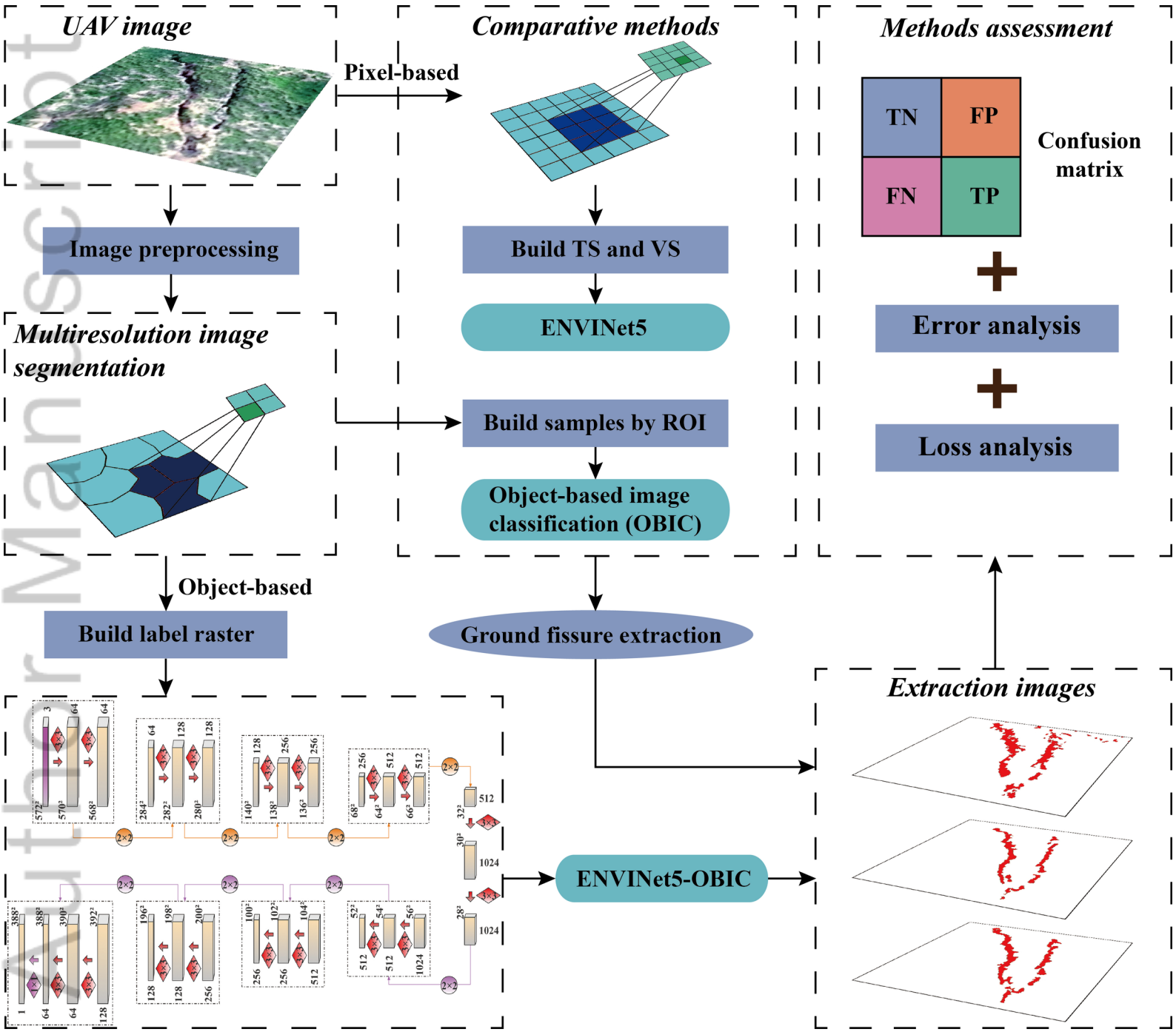

UAV image
Pixel-based
Comparative methods
Methods assessment
TN
FP
FN
TP
Confusion matrix
Image preprocessing
Build TS and VS
ENVINet5
Error analysis
Loss analysis
Multiresolution image segmentation
Build samples by ROI
Object-based image classification (OBIC)
Object-based
Build label raster
Ground fissure extraction
Extraction images
ENVINet5-OBIC

Figure 2.tif

Author Manuscript

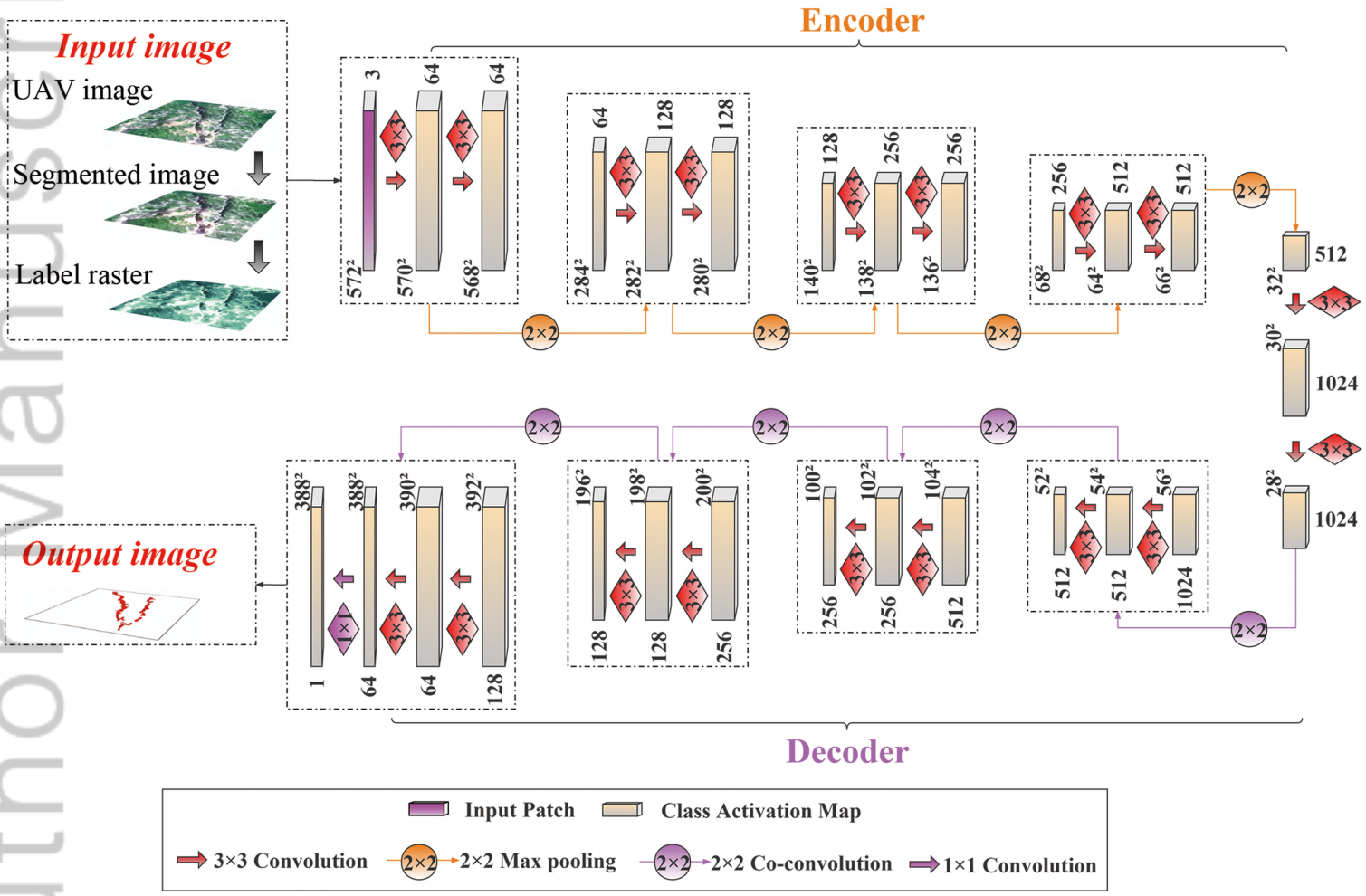
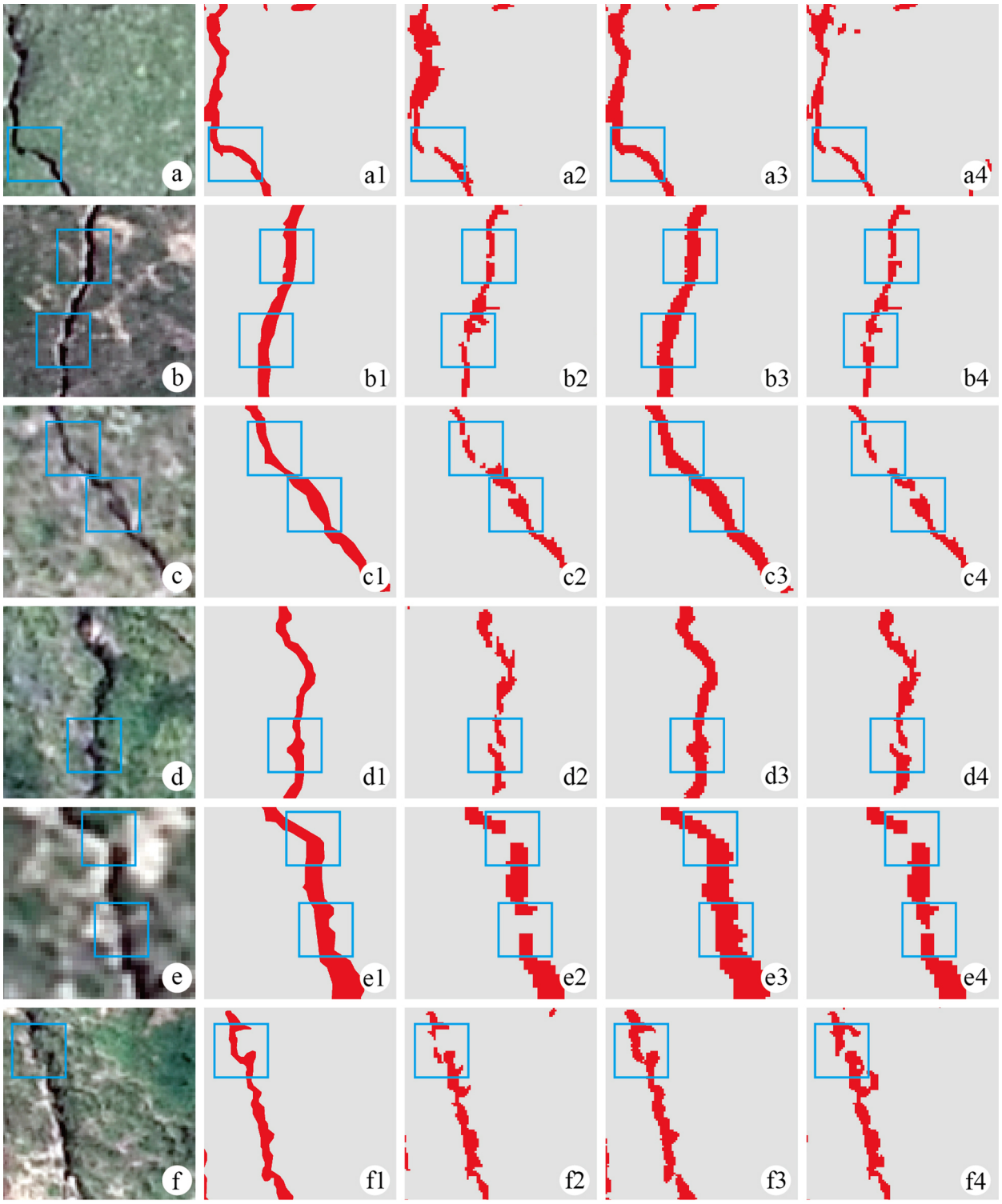


Figure 3.tif

Author Manuscript



Original image | Ground truth | Segmentation scale = 30 | Segmentation scale = 40 | Segmentation scale = 50

Figure 4.tif

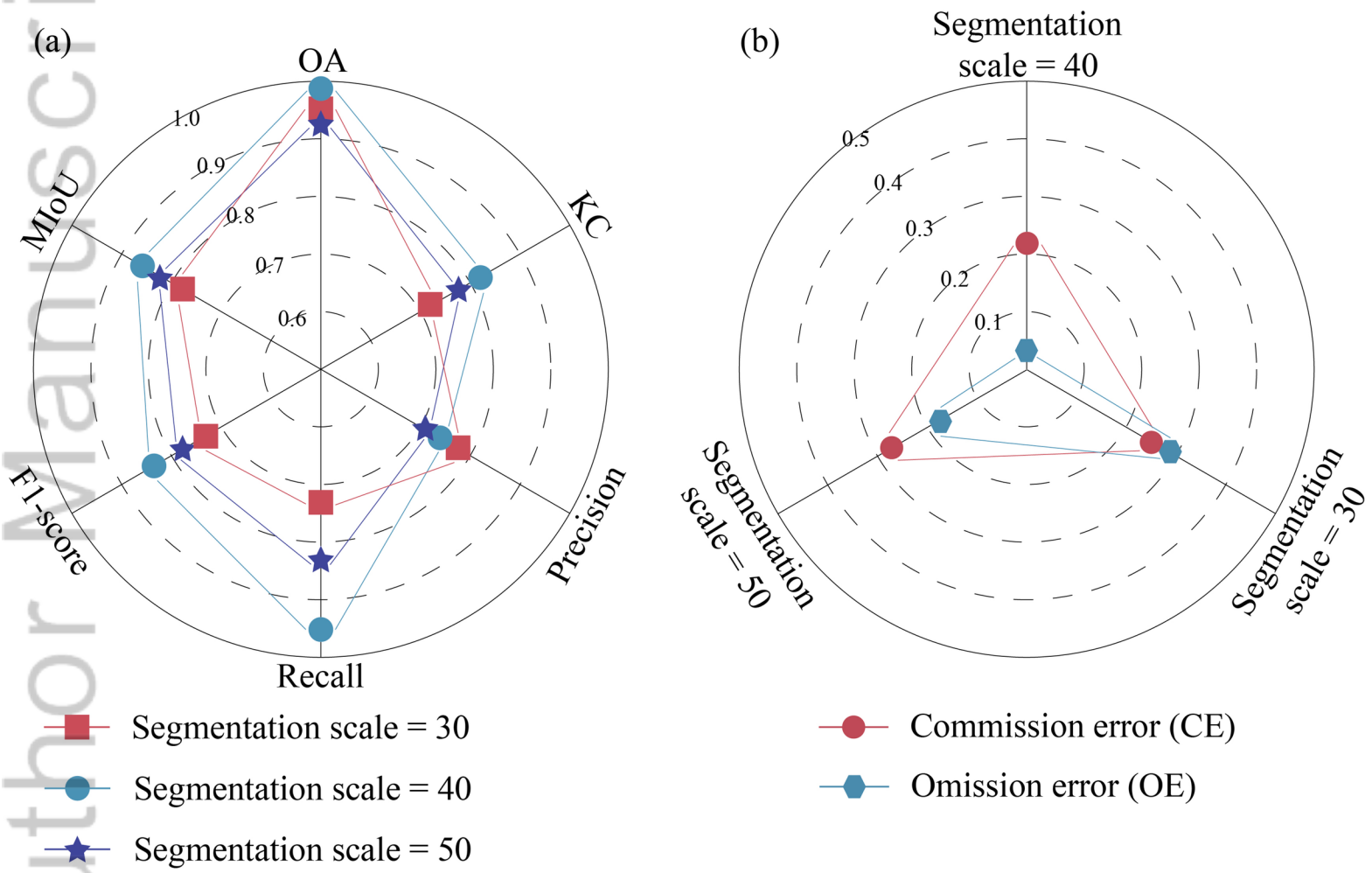
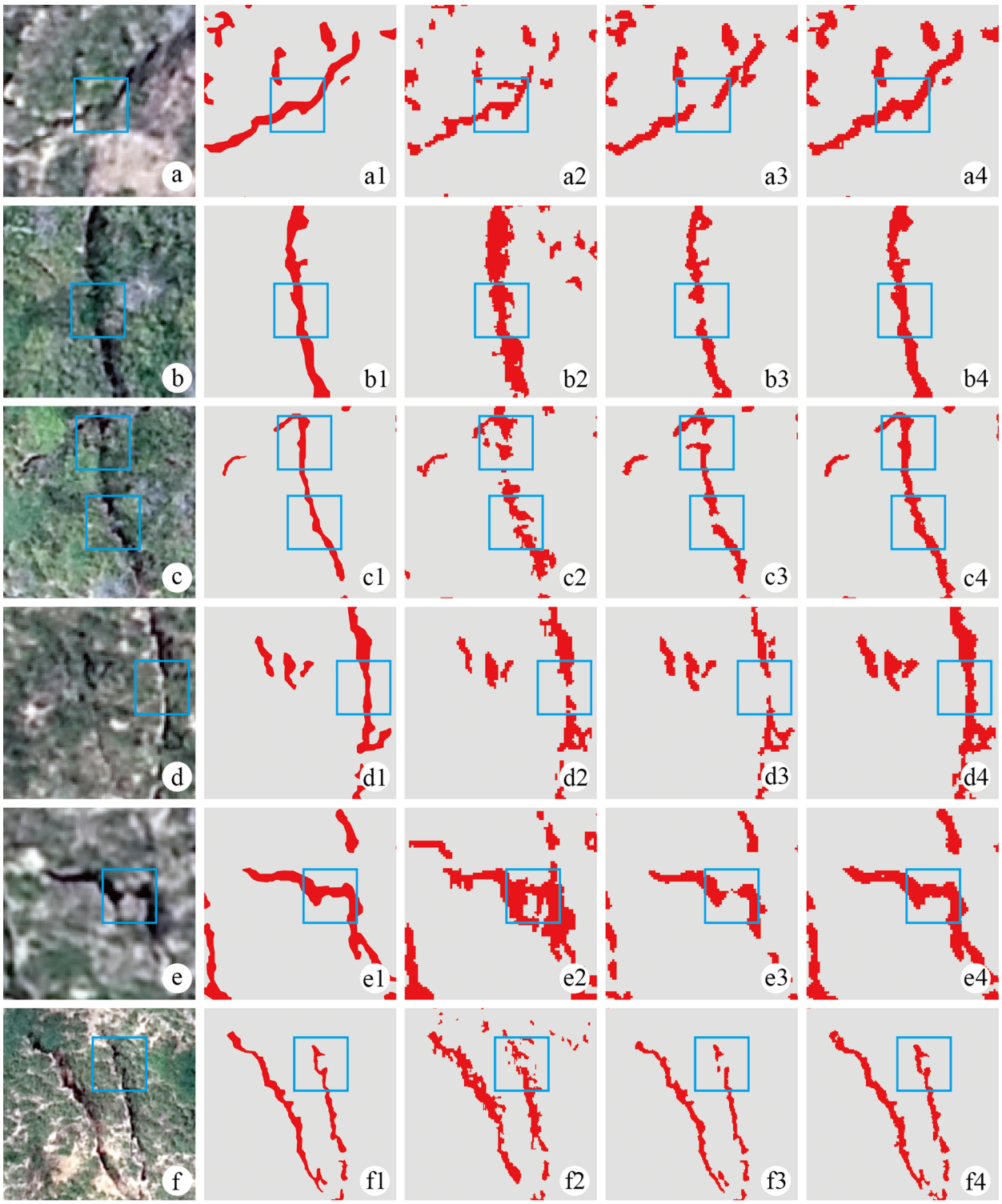


Figure 5.tif

Author Manuscript

Author Manuscript



Original image | Ground truth | Object-based image classification (OBIC) | ENVINet5 | ENVINet5-OBIC

Figure 6.tif

Author Manuscript

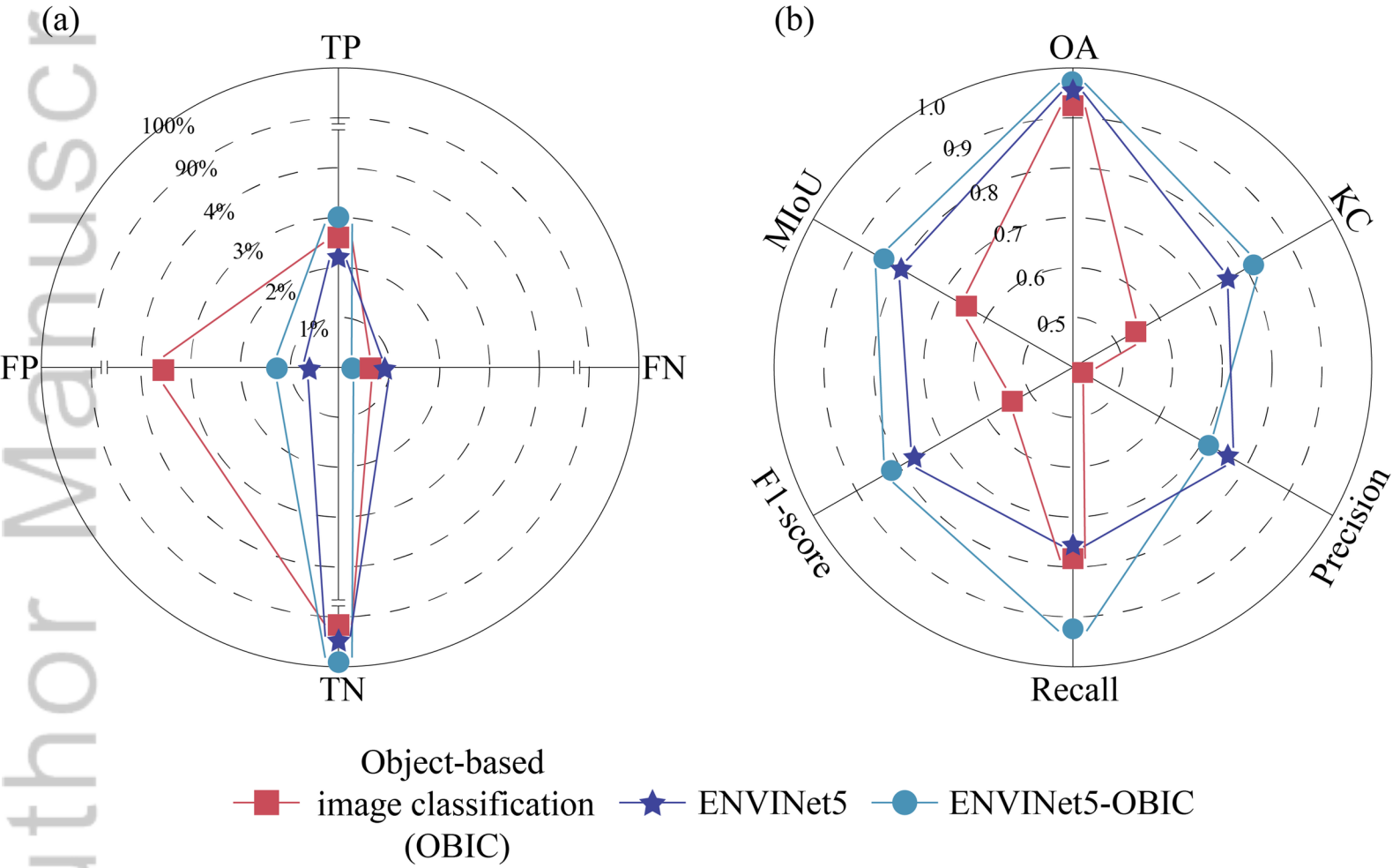


Figure 7.tif

Author Manuscript

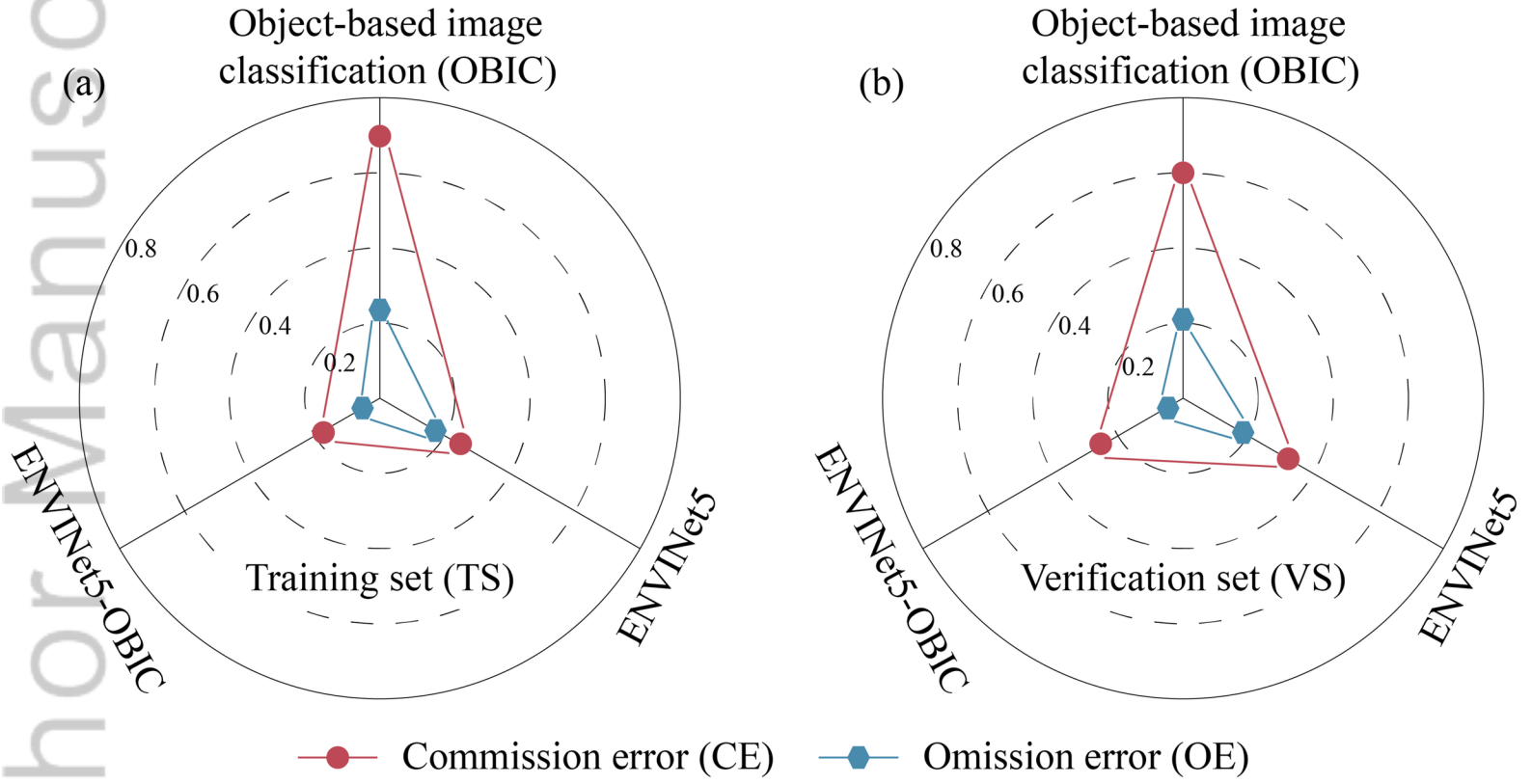


Figure 8.tif

Author Manuscript

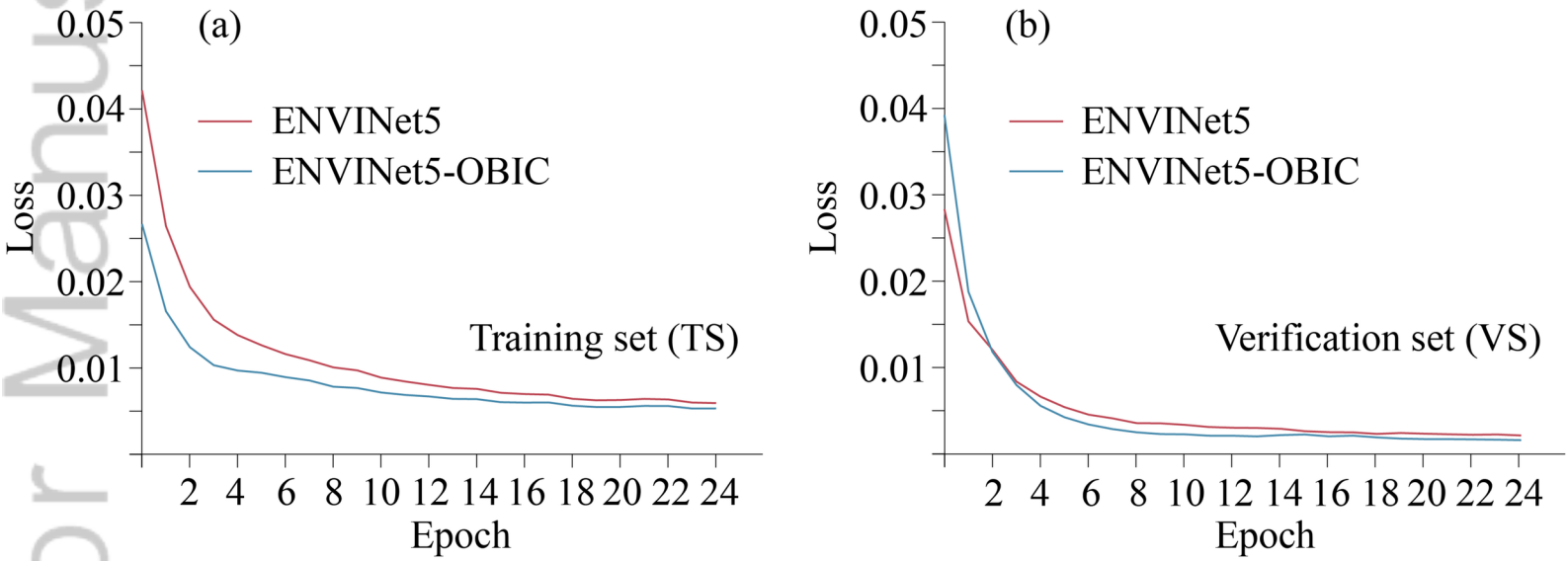


Figure 9.tif

Author Manuscript

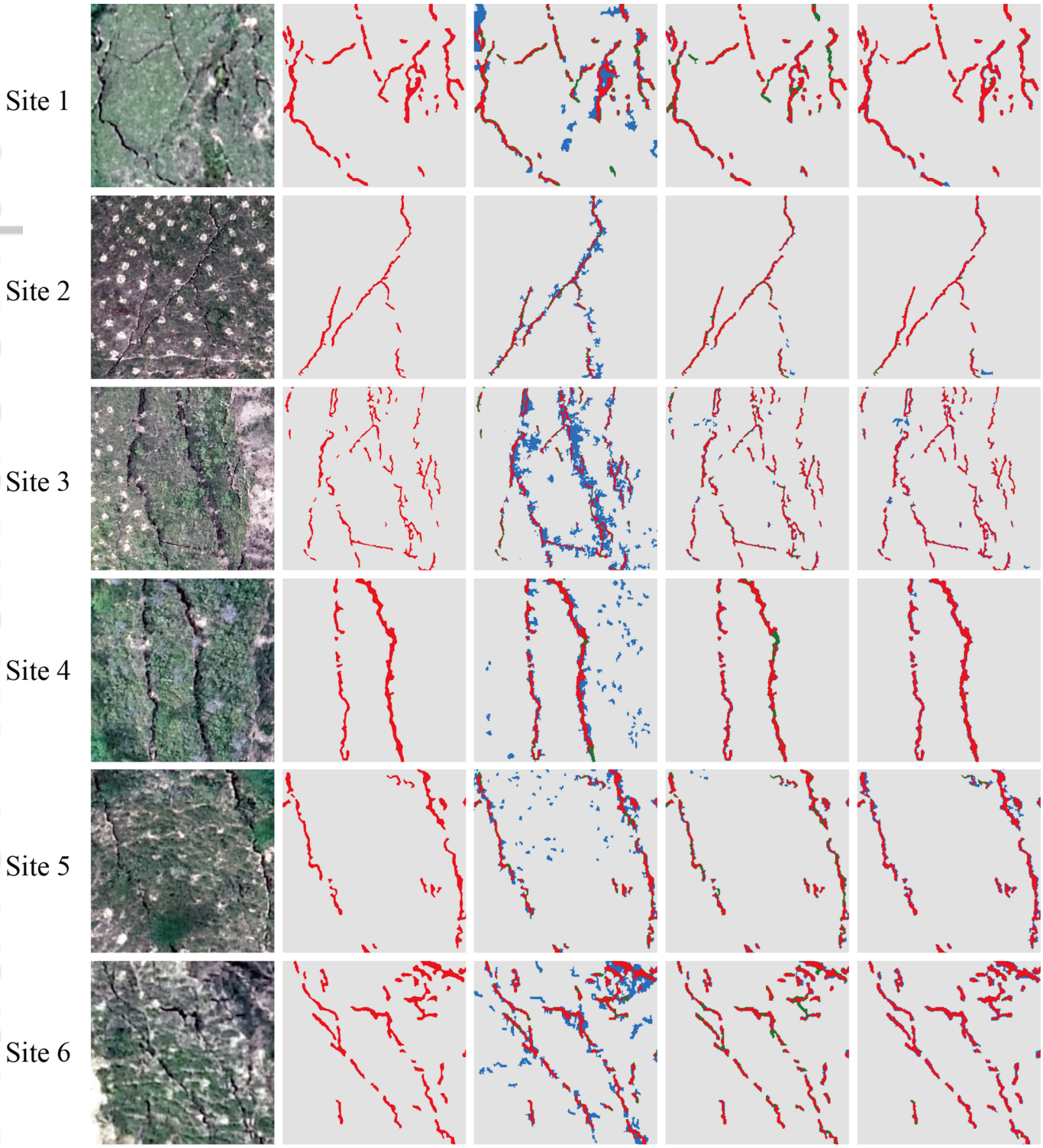


Figure 10.tif

Author Manuscript

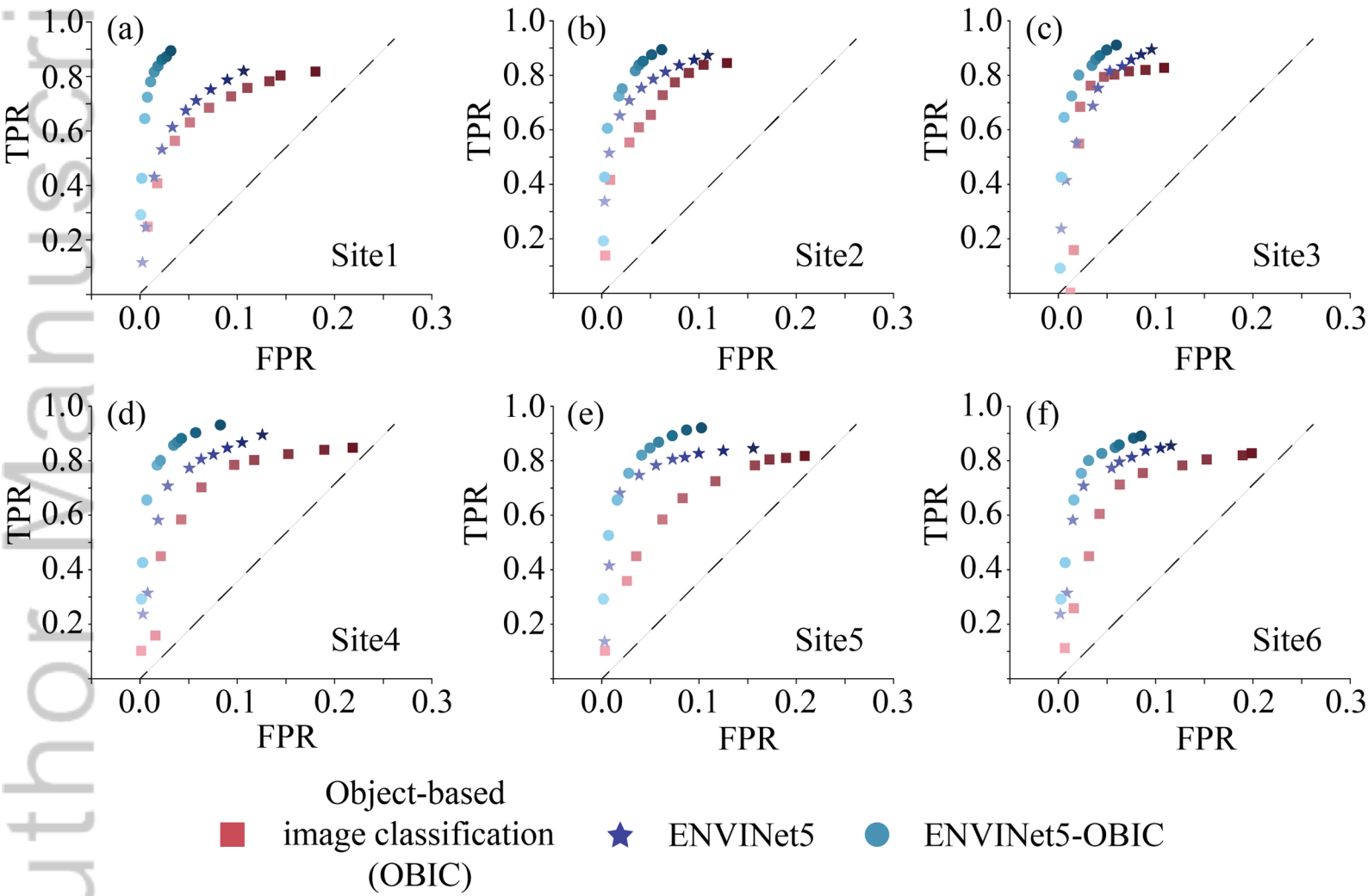


Figure 11.tif

Author Manuscript

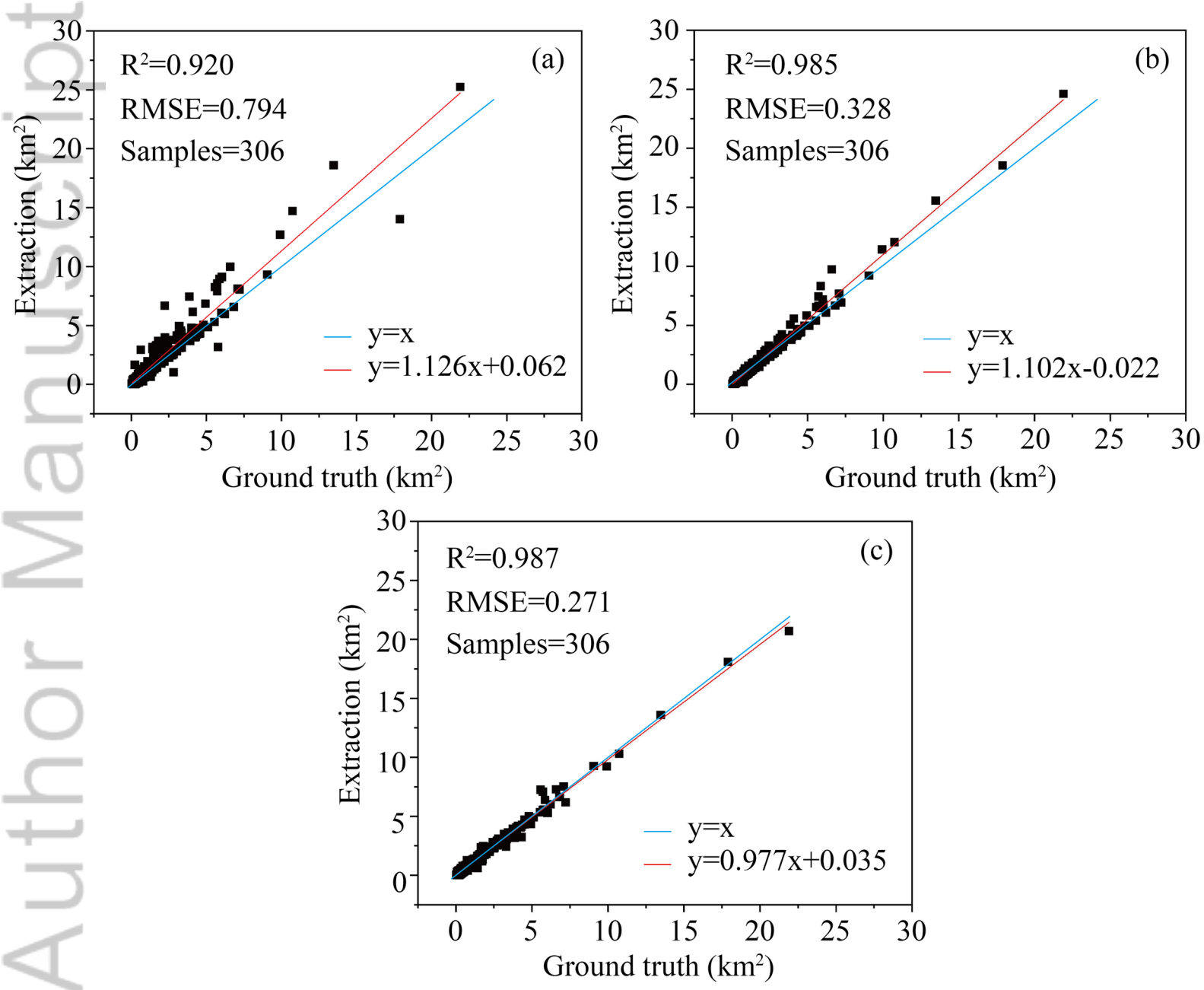


Figure 12.tif

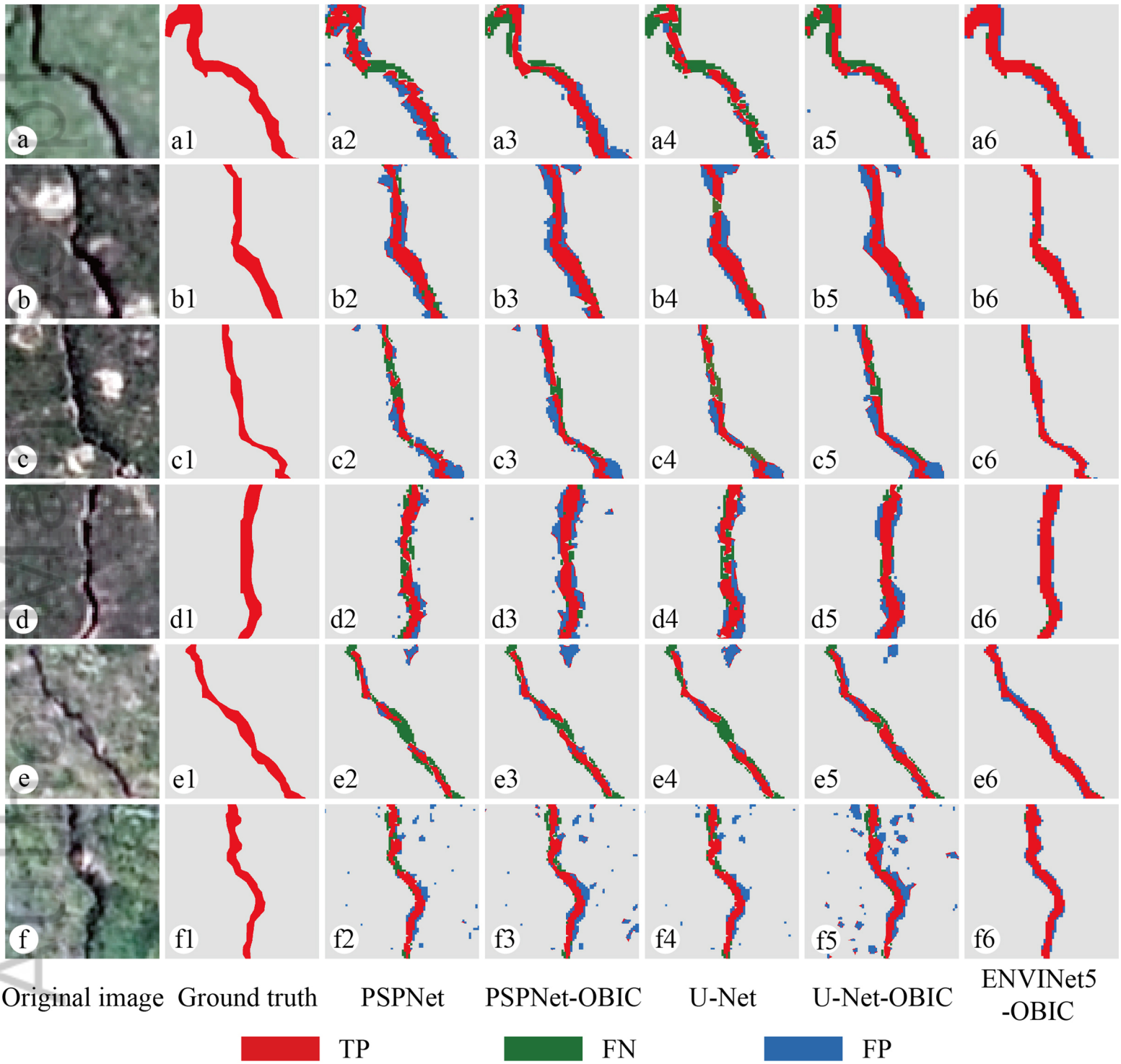


Figure 13.tif

Author Manuscript

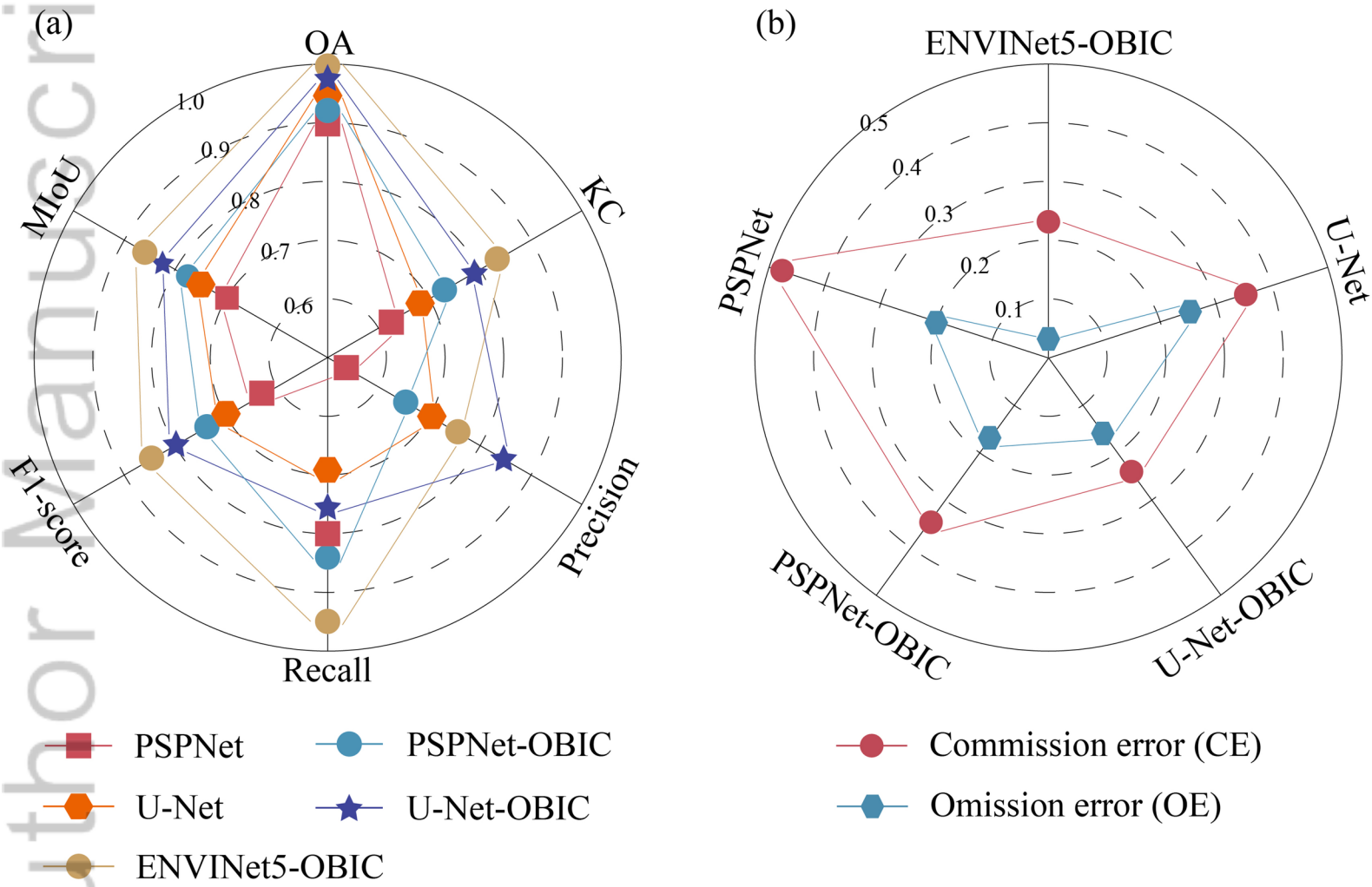


Figure 14.tif